universität wien

MASTERARBEIT

Density functional theory study of oxygen vacancy formation in $LaFeO_3$, $SrFeO_3$, $Sr_{0.5}La_{0.5}FeO_3$

verfasst von

Zeynep Ergönenc, BSc

angestrebter akademischer Grad
Master of Science (MSc)

Wien, 2014

Studienkennzahl lt. Studienblatt:	A 066 862
Studienrichtung lt. Studienblatt:	Masterstudium
Betreut von:	Ao. Univ.-Prof.Dr. Raimund Podloucky

Aileme

Acknowledgements

There are many people who have contributed directly or indirectly to the completion of this thesis, but none is more important than my supervisor, Raimund Podloucky. I couldn't manage having done all this without him. His valuable suggestions, his sense of humor, and wide knowledge of science have inspired me in so many ways, and also have increased both my knowledge and interest in science. Thank you, Raimund, for trusting me when it was trust I most needed. You are a very special person and the best supervisor I could ever have imagined.

Thank you to everyone in the research group, I truly enjoyed each moment I had with all of you. I have always felt that I have and belong to another family here in Vienna. Thank you, René, I could not have survived without our daily conversations and your kind help with any kind of problem I may have had (and a special thanks for when I got stuck in the institute on a rainy day). Thank you for sharing your knowledge, Martin, when I was just starting in a wholly new computational world I truly appreciate it. To Herr Redinger and Herr Herzig, thank you so much for your kindness and willingness to help; to David, Claudia, Marcel, and Cesare, thank you for your support and your great company during my journey.

It was not easy for me to decide what I wanted to do for my masters project, and it is impossible to forget how supportive my supervisor Dr. Anna Laromaine was in my decision while interning at the Institute de Ciéncia de Materials de Barcelona. Thank you, Anna. I will never forget your readiness to help me with decisions for my future, and for always being a very close friend to me.

My enthusiasm in science deeply increased due to the summer school on materials in 3D that I attended at the University of California, Santa Barbara in the early stages of my master thesis. Many thanks to the administrators and presenters for their hard work and dedication.

I also would like to thank my family and friends. To my boyfriend, Erik, thank you for being there: for your love, your friendship and your encouragements. It would not have been the same without you. Katharina, thank you for lovely coffee breaks and lunches. I will definitely be missing the laughter we had in those short breaks. It is impossible to mention to all of my friends here, those who were not directly related to my thesis but certainly made this period of my life more enjoyable and less stressful (you know who you are), I thank you.

It was challenging being away from my family, but they have always made me feel as though they are with me and have always been supportive in any circumstances. Thank you, Mom and Dad; and thank you Sezer, my brother. Thank you for your patience, your love, your care, and for being such beautiful people who I will always admire. I wouldn't be here without you.

Abstract

Perovskite ferrates are of interest as they offer high efficiency for oxygen transport in solid oxide fuel cells which are under consideration for cost-effective and environment friendly electric energy production. First-principles calculations within density functional theory (DFT) as applied in this work, which are free from empirical parameters, are then of particular importance for reliably describing and fundamentally understanding basic physical parameters, such as formation energies of oxygen vacancies, the chemical bonding and related materials properties. The present work demonstrates results of DFT calculations on perovskite ferrates such as $LaFeO_3$, $SrFeO_3$, and $La_{0.5}Sr_{0.5}FeO_3$. A particular problem for DFT modeling of these materials is the localized nature of the Fe-3d valence states which in this work are treated within the so-called DFT+U framework. Tests studies for several types of magnetic orderings were made and a particular choice of the DFT+U parameters was found to be suitable.

The perfect $LaFeO_3$ compound without vacancy was studied extensively also including test calculation for the choice of numerical parameters. Several magnetic orderings including ferromagnetic (FM) and two types of antiferromagnetic (AFM) ordering were investigated and it turned out that the so-called G-AFM ordering is the most stable one for $LaFeO_3$. Different to the La-compound the perfect compound $SrFeO_3$ prefers FM ordering. Consequently, for the mixed case of $La_{0.5}Sr_{0.5}FeO_3$ FM as well as G-AFM ordering were taken into account. The distribution of Sr and La in the mixed compound was studied for two specific choices, which are representative for all possible placements. Depending on the type of AFM larger unit cells have to be constructed. Finally a cell of composition $X_8Fe_8O_{24}$ (X=La, Sr) was taken into account, which allows the study of G-AFM as well as a reasonably small concentration of oxygen vacancies.

The study on single and double oxygen vacancies is treated in the final chapter. Extensive studies on all symetrically different single vacancy sites in G-AFM $La_8Fe_8O_{24}$ were made revealing very costly vacancy formation energies of about 4.2 eV. The situation becomes very different for a single vacancy in $Sr_8Fe_8O_{24}$, which costs only about 0.3 eV. The highlight of the present work is the study of single and double vacancies in the mixed compounds $La_4Sr_4Fe_8O_{24}$ with their two different distributions of La and Sr. In general, the formation energies do not depend strongly on the specific La-Sr distribution but they are much more sensitive to magnetic ordering. For the FM ordering of the mixed case the vacancy formation energies are about 1 eV but they are much smaller for the G-AFM ordering, namely about 0.1 eV per vacancy. There are even cases with negative formation energies, which would mean that the perfect compound is not stable against the liberation of O_2 molecules. Introducing now vacancies the case with G-AFM ordering gets thermodynamically more stable than the mixed case in FM ordering, which is in contrast to the perfect compound. A further interesting finding for the G-AFM ordering with double vacancies is, that the compound is insulating with a

gap larger than 1 eV. This feature corresponds to simple electron counting when all Fe ions have charge +3. Also very interesting is the occurence of a small gap for the FM ordering and two vacancies. This is one of the rare cases of a ferromagnetic insulating or semiconducting material. Summarising, the results on vacancies reveal very intersting physical properties and corroborate from first-principles the experimentally known fact that La-Sr mixed ferrates produce a large numer of vacancies and free oxygen for the transport.

Zusammenfassung

Ferrate mit Perovskitstruktur sind für die Forschung von Interesse, weil sie besonders effizient für den Transport von Sauerstoff in festen Brennstoffzellen geeignet sind. Diese Brennstoffzellen erfreuen sich wegen der Möglichkeit umweltfreundlich und kostengünstig elektrische Energie zu produzieren besonderer Aufmerksamkeit. "First-principles"Rechnungen im Rahmen der Dichtefunktionaltheorie (DFT), wie sie in diser Arbeit gemacht wurden, sind frei von empirischen Parametern. Sie erlauben somit eine zuverlässige Beschreibung und ein grundlegendes Verständnis wichtiger physikalischer Parameter wie Bildungsenergie von Leerstellend und chemische Bindung und damit verbundene elektronische Eigenschaften. Die vorliegende Arbeit zeigt Resultate von DFT Rechnungen für Ferrate mit Perovskitstruktur wie $LaFeO_3$, $SrFeO_3$, und $La_{0.5}Sr_{0.5}FeO_3$. Ein besonderes Problem für die DFT Modellierung dieser Materialien ist die starke Lokalisierung der Fe-3d Valenzzustände, die in dieser Arbeit mit Hilfe der sogenannten DFT+U Methode behandelt werden. Testuntersuchungen wurden für verschiedene magnetische Ordnungen gemacht und daraus geeignete Parameter für die DFT+U Methode ermittelt.

Perfektes LaFeO3 ohne Leerstellen wurde ausführlich untersucht, wobei numerische Parameter getestet wurden. Verschiedene magnetische Ordnungen, die ferromagnetische (FM) und zwei antiferromagnetische wurden studiert. Dabei hat sich heraus gestellt, dass die sogenannte G-AFM Ordnung die energetisch günstigste ist. Im Unterschied dazu ist für $SrFeO_3$ die FM Ordnung am stabilsten. Als Folge dieser Ergebnisse wurden für die gemischte Verbindung $La_{0.5}Sr_{0.5}FeO_3$ beide magnetische Ordnungen berechnet, wobei zwei der möglichen Gitterplatzverteilungen von La und Sr betrachtet wurden. Diese Verteilung ist repräsentativ für alle weiteren möglichen Anordnungen. In Abhängigkeit vom Typ der AFM Ordnung müssen dementsprechend große Zellen konstruiert werden. Zuguterletzt wurden Zellen mit Zusammensetzung $X_8Fe_8O_{24}$ (X=La,Sr) untersucht, die sowohl die G-AFM Ordnung beschreiben können als auch eine vernünftig kleine Konzentration von Sauerstoff-Leerstellen zulassen.

Die Untersuchung von einfachen und doppelten Sauerstoff-Leerstellen wird im letzen Teil der Arbeit vorgenommen. Ausführliche Untersuchungen für alle symmetrisch nicht-äquivalenten Leerstellenplätze in G-AFM $La_8Fe_8O_{24}$ wurden gemacht, wobei eine sehr große Bildungsenergie von 4.2 eV herauskam. Die Situation für FM $Sr_8Fe_8O_{24}$ ist ganz anders, denn in diesem Fall kostet eine Leerstelle nur 0.3 eV. Der Höhepunkt der Arbeit ist dann die Untersuchung von einfachen und doppelten Sauerstoff-Leerstellen in den gemischten Verbindungen $La_4Sr_4Fe_8O_{24}$ mit ihren zwei verschiedenen La-Sr Verteilungen. Im allgemeinen hängt die Bildungsenergie der Leerstellen nicht sehr stark von einer bestimmten La-Sr verteilung ab, aber sie ist sehr empfindlich in bezug auf die magnetische Ordnung. Für FM Ordnung kosten die Leerstellen 1 eV, aber sie sind wesentlich billiger, namlich etwa 0.1 eV, für die G-AFM Ordnung. Für G-AFM gibt

es sogar Fälle mit negativer Bildungsenergie, was bedeuten würde, daß die perfekte Verbindung instabil gegen eine Abgabe von freiem O_2 ist. Führt man nun Leerstellen ein, dann wird die G-AFM Ordnung energetisch gnstiger als die FM Ordnung, was genau das Gegenteil ist zum Fall der perfekten Verbindungen. Ein weiteres interessantes Ergebnis für die G-AFM Ordnung mit zwei Leerstellen ist, dass die Leerstellenverbindung eine relativ große Bandlücke mit mehr als 1 eV hat. Diese Eigenschaft läßt sich mit einem einfachen Abzählen der Valenzelektronen erklären, wenn man annimmt, dass alle Fe Ionen die Ladung +3 haben. Weiters ist besonders interessant, dass für FM mit zwei Leerstellen ebenfalls eine -wenn auch kleine- Bandlücke heraus kommt. Das ist einer der wenigen bekannten Fälle eines ferromagnetischen Isolators oder Halbleiters. Zusammenfassend läßt sich sagen, dass die Untersuchungen an Leerstellen sehr interessante Eigenschaften ergeben haben und die experimentell bekannte Tatsache einer hohen Leerstellenkonzentration La-Sr gemischten Ferraten mit First Principles untermauert werden kann.

Contents

1 Introduction

In the last decade concepts and methods based on Density Functional Theory (DFT) became a very powerful tool for understanding, analysing and even predicting properties of real materials. In this work DFT calculations are presented for perovskite oxides such as $LaFeO_{3-x}$, $SrFeO_{3-x}$, $La_{0.5}Sr_{0.5}FeO_{3-x}$ with varying oxygen stoichiometry. These materials are of interest for the design of solid oxide fuel cells (SOFC) because –as empirically known– the lanthanum-strontium ferrates easily provide oxygen ions for transporting charge. This work is embedded in the Special Research Branch (SFB) project "FOXSI" [1] on Functional Oxide Surfaces and Interfaces sponsored by the Austrian Science Fund FWF.

The DFT modelling, which can be made free from empirical parameters (i.e. from first principles), has particular importance for describing and fundamentally understanding the thermodynamic stability and electronic structure of materials. As is known for transition metal oxides the metal orbitals (in our case: d-orbitals of Fe) become strongly localised and have to be treated in a manner beyond the standard approximations as implemented in all the DFT codes. The special treatment was done by means of the so-called GGA+U method in order to decribe properly the magnetic ordering and size of the gap in the electronic structure. It combines the standard approximation for the manybody part of the electronic interactions based on the homogenous electron gas in terms of the Generalized-Gradient- Approximation (GGA) with an atomic-like description for the Fe-d orbitals.

One very important aspect concerning thermodynamical stability as well as the electronic structure is the magnetic ordering. Due to the localised unfilled d-orbitals the Fe-atoms carry local spin magnetic moments, which may be ordered in a simple parallel way (ferromagnetic, FM) or in some anti-ferromagnetic (AFM) arrangement, which results in physically different Fe atoms. Therefore, spin-polarised calculations have to be done for suitable large supercells modelling selected AFM orderings.

2 Solid State Electrodes

Solid Oxide Fuel Cells (SOFCs) are batteries which produce energy through electrochemical reactions. They need hydrogen to run, but the direct use of hydrocarbon fuels, such as methane, is also possible [2], [3], [4]. As it is shown in Fig. 1, oxygen gas is introduced from porous cathode and hydrogen gas applied from a porous anode, which encounter oxide ions producing water and energy. SOFCs are environmental friendly, and promising for efficient, sustainable energy production in the future [5] but they are not ready for technological applications, and research is strongly going on to design robust, efficient SOFCs. The major problem is as to which the high potential of the oxygen reduction reaction at the cathode side,

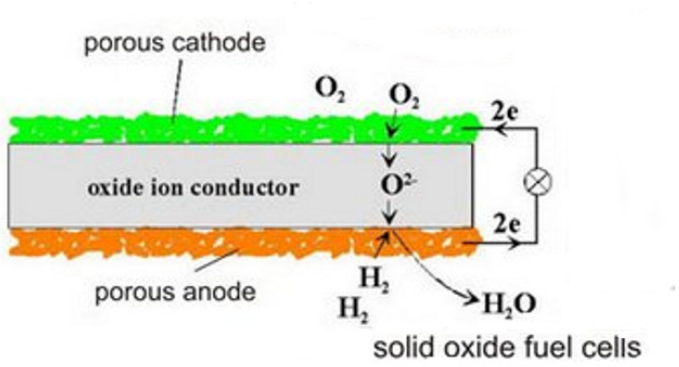

Figure 1: Scheme of oxygen transport in a solid oxide fuel cell [1].

which requires expensive catalyst and can be overcome by high operating temperatures [6]. However, high temperatures cause cathode materials to age faster [7] and also are not very useful for portable devices. SOFCs work as simple as it is shown in the Fig. 1. However, it is also surprisingly complex. The electrocatalytic decomposition of oxygen, fast oxygen diffusion and temperature affects are still of a research and very challenging to develop a SOFCs to be easily used in the markets. Current studies show that mixed ion and electron conducting materials (MIEC) are enhancing the oxygen diffusion and surface exchange rate, therefore the oxygen reduction reaction [8] [9] [10].

Researches in this field has shown that the energetic of oxygen vacancy formation has a key role on bulk diffusion in ABO_3 perovskite type oxides. A very important study has been demonstrated by Carter *et al.* shows that near zero oxygen vacancy formation energy performs high oxide ion diffusion in the MIEC materials [11]. Consequently, it is important to facilitate the oxygen formation energy, to enhance the MIEC materials in SOFCs [12]. That is the point for which La-Sr-Fe perovskite oxides and the oxygen vacancy formation energies thereof are of high interest and importance.

The atomic electronic configuration of La (atomic number: 57) is [Xe]$5d^1 6s^2$, and its oxidation states vary between +2 to +3. The atomic electronic configuration of Fe (atomic number: 26) is [Ar]$3d^6 4s^2$ and its most common oxidation states are +2 and +3, other oxidation states such as -1, 0, +1, 4 and +6 are rare but exist [13]. Strontium (atomic number: 38) with electronic configuration [Kr] $5s^2$. As discussed later on $SrFeO_3$ contains Fe with the high-oxidation state of +4 [14]. The atomic electronic configuration of O (atomic number: 8) is $1s^2 2s^2 2p^4$ and its most common oxidation state is -2, because then the $2p$-shell is filled. O is very electronegative, 3.44.

When La, Sr, Fe and O form solid compounds ABO_3 compounds with the perovskite structure. In this structure the B ions are surrounded by 6 oxygen ions and has octahedral co-

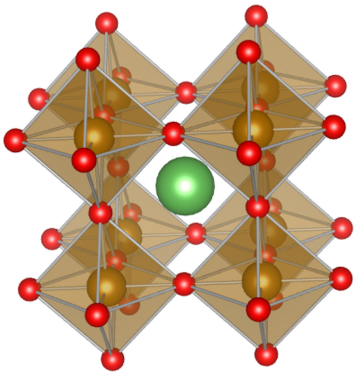

Figure 2: Sketch of crystal structure of the cubic perovskite oxide ABO_3. T shows the octahedral configuration of oxygen (red spheres) and the positons of the A (green spheres) and B cations (yellow spheres).

ordinations, as sketched in Fig. 2. It should be noted that the sketch shows a high-symmetry arrangement. In general, the ideal cubic structure is distorted resulting in a rather large number of possible preovskite structures. Stoichiometric deficiencies are quite common in perovskite oxides and they can occur either at the cationic sites as well as on the oxygen sublattice. In this thesis, oxygen deficiencies or vacancies in $LaFeO_3$, $SrFeO_3$, and Sr-$LaFeO_3$ were studied.

3 Magnetic Ordering

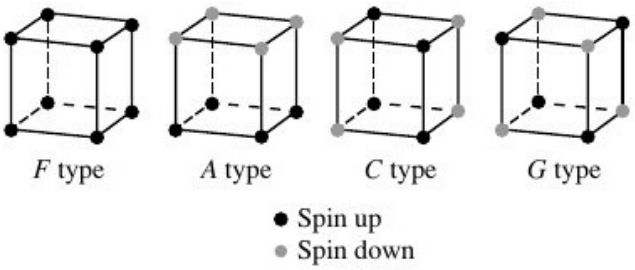

Figure 3: Ferromagnetic (F) and the itwo most important antiferromagnetic spin orderings (A type, G type) on the iron sublattice [15].

As mentioned in the introduction, spin orderings are of crucial importance for the thermodynamic stability, since they strongly influence the total energy of the ferrates. For these large-gap oxides a special treatment of the Fe d-like states is needed, because they are strongly localized and the gap comes out too small when standard approximations to the

exchange-correlation DFT functional are applied. As elaborated later on this will be done by adding atomic-like electron correlation and exchange interactions in terms of the parameters U and J, respectively. The choice of these parameters crucially influences the stability of a given spin arrangement. Fig. 3 depicts three types of magnetic ordering, one ferromagnetic (FM) and the two most common anti-ferromagnetic (AFM) orderings. The A type consist of alternating FM planes perpendicular to one of the main axes, whereas for the G-type ordering alternating FM planes are stacked in along the [111] direction. Technically, one has to start within DFT when solving the self-consistent Kohn-Sham equations one has to start with a certain assumption of orderings of local moments with given size, which might even lead to a change of ordering or even breakdown of local moments. This does not happen in the present cases, the chosen ordering is rather robust and is usually maintained until convergency has been reached. This certainly has to do with the choice of rather large U-J parameters (usually: 6V). The AFM orderings shown in Fig. 3 of course need large unit cells, the sketches only serve as illustrations. Suitably large supper cells have to be chosen (see later on), which are anyway needed for the study of oxygen vacancies. It should be noted, that also oxygen atoms could carry around small but distinctive local moments, which is due to polarization effects of the Fe atoms in the centers of the octahedrons formed by the O atoms. One technical remark concerning the local moment: its definition is somewhat arbitary because -strictly speaking- in a solid the atoms loose their identity. Nevertheless, for understanding and analysis purposes one ascribes local properties to atoms, which can be done e.g. by circumscribing a sphere with some reasonable radius around each atom. Then, all quantities derived within this atomic spheres are then defined to be a local property of this particular atom. In the present work, the radii were chosen as given in the POTCAR file, namely 1.164 Å for Fe and 0.820 Å for O (parameters RWIGS).

4 Computational Aspects

4.1 Density Functional Theory

DFT is presently the most succesful concept for solving Schrödinger's equation in computational materials science. In the last decade in particular the number of publications is almost exponentially increasing. Its success as a first-principles method is based on its universality, flexibility and the treatment and approximation of the electronic many-body interactions. In many cases materials properties can derived in a reliable way and it is able to predict, corroborate and analyze experimental results. Briefly, the most basic equation of DFT is [16] The total energy E of the ground state is a functional of the ground state density $n(\mathbf{r})$ in which $\mathbf{r}$

comprises space- as well as spin coordinates,

$$\mathrm{E}[n(\mathbf{r})] = \int [n(\mathbf{r})]\mathrm{V}_{\mathrm{ext}}(\mathbf{r})d\mathbf{r} + \mathrm{F}[n(\mathbf{r})]. \tag{1}$$

The first term describes the classical Coulomb interaction of the electron density with the so-called external potential which for the present purpose is the Coulomb potential generated by the atomic nuclei. The functional F includes the classical Coulomb interactions as well as the quantum many-body interactions $\mathrm{E}_{xc}[n(\mathbf{r})]$ referring to exchange and correlation. DFT was applied in its usual computational convenient formulation, namely in terms of the self-consistent Kohn-Sham equations [17]. The basic concept there is to map the many-body system onto a fictitious single-particle system. By that, auxiliary orbitals are introduced which are the eigensolutions of self-consistent Schrödinger-like equations, the Kohn-Sham equation. The potential energy there is decribed as the effective potential V_{eff},

$$\mathrm{V}_{eff} = \mathrm{V}_H + \mathrm{V}_{xc} + \mathrm{V}_{ext}, \tag{2}$$

which consists of the Hartree-like classsical Coulomb potential of the density, the external potential as generated by the nuclei and the exchange-correlation potential which comprises all non-classical (i.e. quantum) interactions. The direct connection to DFT is given by the role of the Kohn-Sham orbitals: their only meaning is that, when squared and properly summed up they build up the exact ground state density. So far, no approximations have been made assuming that the mapping of the many-body system onto the fictitious single-particle framework exists mathematically, which was proven in many papers at the beginning of the success-story of DFT as applied in its Kohn-Sham form.

For real systems, $\mathrm{V}_{ext}[n(\mathbf{r})]$ has to be approximated. The whole succes of DFT (which finally resulted in the Nobel prize for Walter Kohn and John Pople, the Gaussian founder) is based on the usefulness of simple and computationally fast approximations as derived from properties of the homogenous electron gas. By that, locally at each point the value of the "true" density is taken as the density of the homogenous electron gas, for which the exchange-correlation interactions can be calculated. The most simple of such a *local* approximation is the so called local-density-approximation (LDA). A more refined but still very fast approximation is the so-called generalized gradient approximation (GGA) taking into account also the gradient of the exchange-correlation functional with respect to the ground state density. In this work the parametrization of Perdew, Burke and Ernzerhof (PBE) [18] is applied.

4.2 Vienna Ab-initio Simulation Package (VASP)

For the actual calcuations the DFT code VASP is used. VASP stands for Vienna Ab-initio Simulation Package. It uses a plane wave basis set with periodic boundary conditions and the projector augmented wave method (PAW), developed by P. Blöchl [19] for constructing the pseudopotentials. It was and is developed in computational material physics department at the University of Vienna by Kresse [20] [21] [22]. It has been widely used in theoretical researches all over the world.

VASP uses four basic input files; INCAR, POSCAR, KPOINTS, POTCAR and important output files OUTCAR, CHGCAR and DOSCAR files. The POSCAR file contains the geometry parameters (i.e. basis vectors, atomic positions and related information). The POTCAR file provides the pseudopotential for each atomic species, and it has to be chosen according to the exchange-correlation approximation (GGA or LDA) and its "hardness", i.e. how many core-states are taken into account. The file KPOINTS informs VASP about how to construct the k-points mesh [23]. INCAR contains control parameters for all of the features of VASP.

4.3 LDA+U/GGA+U

As mentioned the standard approximations for the exchange-correlation functional of DFT application are based on the homogenous free electron gas. Clearly, once the true density deviates strongly from a constant value then the failure of LDA and GGA becomes significant in particular for describing features of the electronic structure such as magnetic moments and stability of magnetic orderings, the band gap as well as the total energy. i.e. the stability of a certain phase. The more localized states are, the larger the error. A typical example for strong(er) localization are the d-states of transition metal elements in an oxide environment, such as $XFeO_3$, as studied in the present thesis. There is a variety of cheaper and very expansive developments beyond LDA and GGA (so-called post-DFT functionals). One of these concepts, the so-called namely the GGA+U method, is used for the calculations of this thesis. By that, the d-states of Fe are considered to be localized in spheres with a given radius (RWIGS in the INCAR or POTCAR file) and treated in an atomic-like manner, by which the manybody iteraction are included in terms of a Coulomb parameter U and exhange parameter J. Here, a model version is used in which only the difference of U-J matters [24]. This procedure is chosen by setting the parameter LDAUTYPE=2 in the INCAR file. Traditionally, J is fixed to 1, therefore when one speaks about an $U=U_0$ calculation, the effective parameter entering the calculations is U_0-1.

5 Results of DFT calculations

5.1 Total energy in the Kohn-Sham formulation

DFT as formulated by Kohn-Sham [17] has been used to calculate the total energy of the ground state for a given distribution of atoms. The results in the present work are free from any empirical geometry input, which clearly shows the advantages of the theory. The geometry is optimised by minimizing the atomic forces as well as the volume to find a cell shape and atomic arrangement where the molecule is more stable. The total energy of the electronic system is calculated according to

$$E_{tot,el} = \sum_{i}^{N} \varepsilon_i - \frac{1}{2} \int \int \frac{\rho(\mathbf{r})\rho(\mathbf{r}')}{|\mathbf{r}-\mathbf{r}'|} d\mathbf{r} d\mathbf{r}' + E_{xc}[\rho] - \int v_{xc}(\mathbf{r})\rho(\mathbf{r}) d\mathbf{r} \tag{3}$$

summing over all N occupied states, correction is needed for the double counting of the Coulomb interaction, adding the exchange-correlation energy functional E_{xc} and final subtracting the corresponding expression involving the exchange-correlation potential $v_{xc} = \delta E / \delta \rho$, which is the functional derivative of E_{xc}. For periodic boundary conditions the sum $\sum_i$ is replaced by the sum $\sum_{\mathbf{k},\nu}$ involving a vector of the first Brillouin zone $\mathbf{k}$ and the band index ν. So far the total energy of the electronic system has been derived. For the total energy of electrons and nuclei the Coulomb repulsion of the nuclei α with charges Z_α has to be added according to

$$E_{tot} = E_{tot,el} + \sum_{\alpha>\beta} \frac{Z_\alpha Z_\beta}{|\mathbf{r}_\alpha - \mathbf{r}_\beta|} \tag{4}$$

E_{tot} is now minimised for each geometry of nuclei according to the construction of the Kohn-Sham equation. Furthermore. E_{tot} can also be minimised with respect to the atomic distribution (i.e. positions and cell volumes) which includes the minimisation of forces acting on the atoms.

5.2 Electronic structure and density of states

The density of states describes the energy distribution of the Kohn-Sham equations according to relation [17]. The distribution of energy levels around Fermi energy is of interest, which is expressed by the density of states (DOS) $n(E)$. The definition is straightforward: number of levels with precisely the energy E,

$$n(E) = \sum_{i,\vec{k}} \delta(\varepsilon_{i,\vec{k}} - E) \tag{5}$$

We sum over all states labelled by the quantum numbers $i, \vec{k}$ according to the periodic boundary conditions. The δ-like function gives 1 if the argument is zero (i.e. $\varepsilon_{i,\vec{k}} = E$) and 0 otherwise. If we use a continous $\vec{k}$-space, then the $\vec{k}$-sum is transformed into an integral,

$$n(E) = \frac{1}{\Omega_B} \sum_i \int d^3\vec{k}\, \delta(\varepsilon_{i,\vec{k}} - E). \tag{6}$$

Now, $\delta(arg)$ is the true distribution "function": 0 if $arg \neq 0$ and ∞ for $arg = 0$. It is defined via the mathematical definition, $f(x_0) = \int_{-\infty}^{+\infty} f(x)\delta(x - x_0)\, dx$. The normalization volume Ω_B is the volume of the first Brillouin zone defined by the inverse of the volume of the unit cell Ω,

$$\Omega_B = \frac{(2\pi)^3}{\Omega} \tag{7}$$

[25]

For analysing the DOS quite often the concept of the so-called local DOS is used: to each atom a sphere with a given radius is attributed and the locale DOS is then derived by integrating over the atomic sphere. In this way the total DOS can be split into contributions originating from each atom. Furthermore, inside the atomic spheres all quantities such as the local DOS can be expanded into spherical harmonics thereby labeling the contributions with l-quantum number referring then to an s-, p- or d-like character. These DOS contributions are called partial DOSes. The local partial DOSes are helpful for understanding the atomic characteristic of states. The radii used are contained in the POSCAR of each atom as used by VASP.

For summing over occupied states the DOS has to be multiplied with the the Ferm-Dirac distribution function

$$f(\varepsilon, T, \mu) = \frac{1}{e^{\frac{\varepsilon - \mu}{kT}} + 1} \tag{8}$$

The chemical potential μ at $T = 0$ corresponds to the Fermi energy E_F, which is then the energy of the highest occupied state. For semiconductors at finite temperatures the chemical potential must be in the gap in order to derive the correct number of occupied states.

6 Perfect Structures

6.1 Ferromagnetic cubic $LaFeO_3$

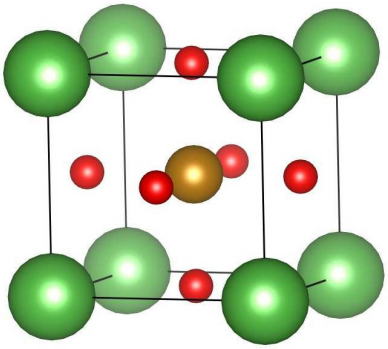

Figure 4: Sketch of the most simple cubic crystal structure of perovskite $LaFeO_3$ consisting of 5 atoms per unit cell. Color coding of positions is: green La, yellow Fe and red O atoms. This most simple perovskite structure is a combination of an fcc and bcc lattice. Note the octahedron formed by the Fe ions with O in its center (See Appendix 9.1).

As a preliminary step to the actual investigations a series of test calculations have been performed in order to check computational parameters and to gain expertise with the system. As shown in Fig. 4 the simplest possible perovskite unit cell consists of 5 atoms referring to cubic Lanthanum orthoferrite with FM magnetic ordering of the Fe atoms. Tests were made with respect to a) the convergency of total energy with respect to the basis-size (see Fig. 5) and the **k**-point grid (see Fig. 6) and b) the equilibrium volume as derived from the minimum of the total energy. On the basis of the results in Figs. 5 and 6 an energy cut-off 480 eV and an $8 \times 8 \times 8$ **k**-point grid was considered to be sufficiently accurate for the 5-atoms unit cell. KPOINTS has the information about the k-point meshes which should be found by plotting the relation energy versus several k-point meshes until the energy converged. For these choices an absolute error of the total energy with respect to convergency is expected to be ≤ 0.15 meV per atom.

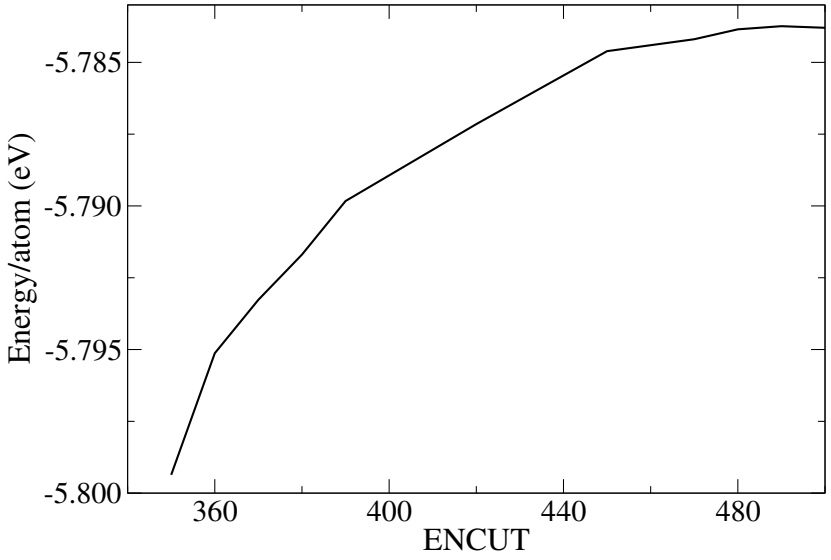

Figure 5: Total energy vs. energy cut-off for studying the basis-set convergency. Exchange-correlation approximation according to PBE [18].

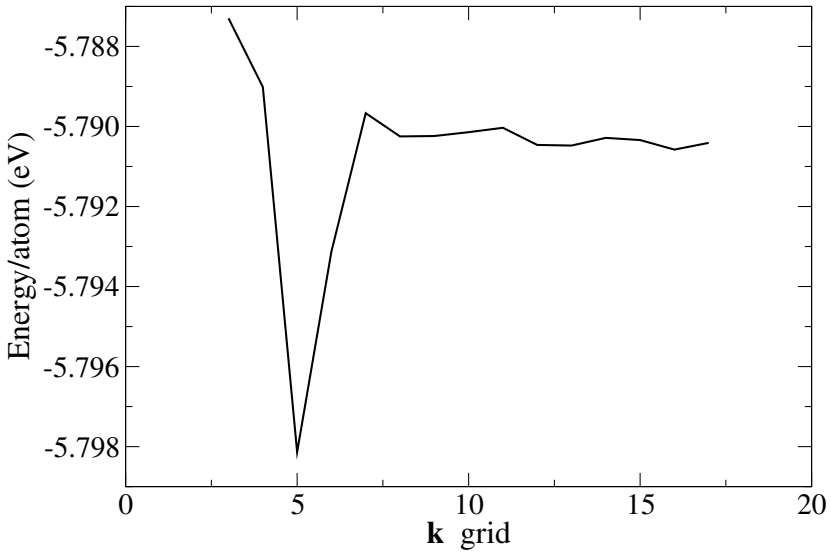

Figure 6: Total energy per atom vs. **k**-point mesh. Mesh construction according to Monkhorst and Pack [23]. Integration method according to VASP parameter, Gaussian smearing (ISMEAR=0) with half-width SIGMA=0.05 eV. [29] Energy cutoff: 480 eV. PBE potential.

It should be noted that DFT as it is used in calculations like the one in the present work refers to the electronic system at T=0K because no excitations are taken into acccount in the

exchange-correlation functionals and its approximation. Within the single-particle framework of the Kohn-Sham theory one could easily include temperature via the smearing of the Fermi-function (see Chapter 5.2) or some other type of smearing as introduced in the **k**-point sampling.

After optimizing the energy cut-off and the **k**-point set the equilibrium volume was searched for. This is done by minimizing the total energy $E_{tot}(V)$ as a function of volume V or lattice parameter in the cubic case as presented in Fig. 7. It shows a very smooth curve which proves the stability and accuracy of the VASP calculation. It can also be seen, that not far away from the minimum $E(V)$ starts to deviate significantly from a parabolic behaviour. The cubic equilibrium lattice parameter for FM $LaFeO_3$ is given in Table 1 showing also its dependency on the Coulomb parameter U. According to the neutron diffraction study by Koehler and Wollan [31] the lattice parameter of $LaFeO_3$ in the GAFM ground state was found to be $a = 3.93$ Å for the volume of one formula unit, and T. Koubský [30] calculated a value of $a = 3.94$ Å from his GGA+U with U=6 study. This values are very close to the result in Table 1 of 3.95 Å for U=6 eV.

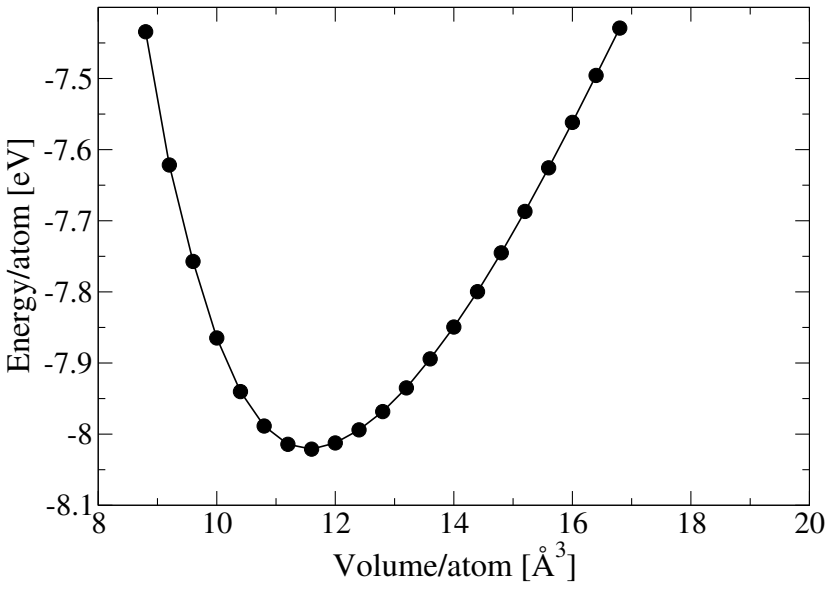

Figure 7: Total energy per atom of ferromagnetic $LaFeO_3$ with the 5-atom cubic perovskite structure energy vs volume per atom.

The spin split density of states (DOS) as calculated with the PBE potential is of the FM ordering is shown in Fig. 8. There, one observes a significant hybridization of Fe d-like states and O p-like states in particular for the majority spin states below -5 eV and around -2 eV. Clearly, due to hybridization the spin-split O-like states become unsymmetric indicating some induced local magnetic moment as listed in Table 1. In particular around

Fermi energy E_F one observes mostly spin-down Fe states with rather weak hybridization. The two main peaks of spin up and down states around E_F are split by about 2.5 eV indicating the exchange splitting of the GGA-PBE functional. The large peak of the La DOS at about 2 eV is attributed to the unoccupied f-states. Fig. 8 does not show any gap resulting in a metallic character of the system.

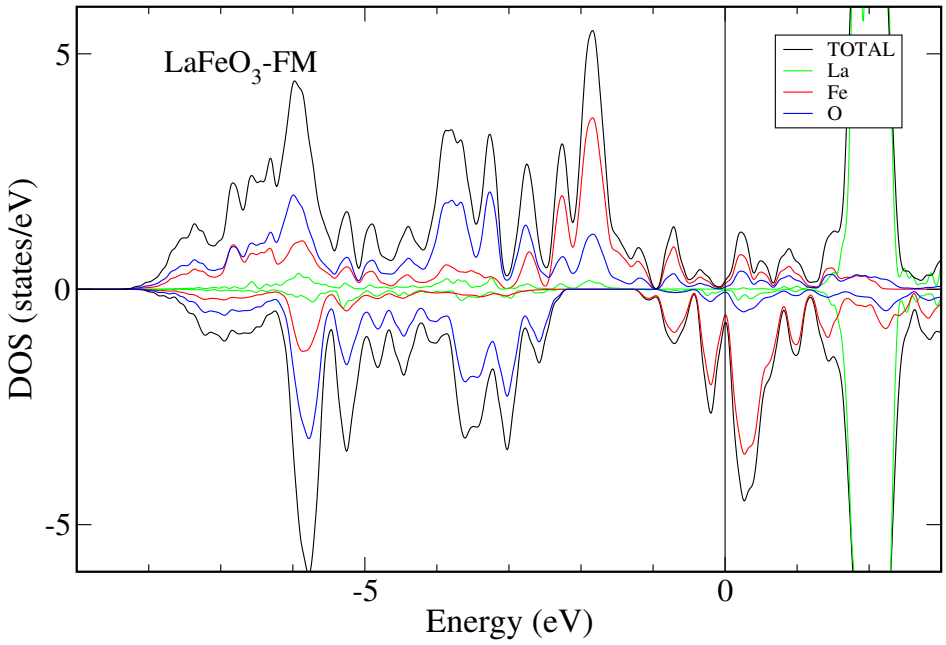

Figure 8: Spin polarized total and local density of states of ferromagnetic $LaFeO_3$ in the 5-atom perovskite unit cell with the PBE potential. Positive/negative values: spin up/down contributions. Fermi energy at E=0.

It is well known that a standard DFT treatment of transition metal oxides with unfilled 3d orbitals like $LaFeO_3$ show rather large failures due to the local approximation as applied in LDA and even GGA. Effects of strong localization have to be included in some more or less fancy way. In the present study this is done by the so-called LDA/GGA+U method as described in Chapter 4.3. As mentioned in this chapter, speaking about a certain value of U actually means that the effective parameter U-J with J=1 eV is taken for the VASP calculation. Table 1 shows the results of VASP calculations with PBE and U=2, 4 and 6 eV. It can be seen, that the larger the U the less negative (i.e. less bonding) the total energy gets because U represents a Coulomb repulsion. Also the local moment of Fe increases due to the stronger localization of the d-states. The same happens for the local moment of O which nicely demonstrates the polarization effect of the surrounding strongly polarized Fe atoms. It seems, however, that some saturation is reached for U=6 eV, because the increase

of the local moment when compared to U=4 eV is only 0.18 μ_B. This is quite different when compared to the change of 0.9 μ_B when U is increased from 2 to 4. The maximum of the local moment would be 5 μ_B if Fe only has 5 filled 3d states which are all perfectly localized in the given atomic sphere defined by the RWIGS parameter in the POTCAR. Also the equilibrium volumes increase with increasing U, but -again- it reaches saturation for U=6 eV.

Concerning the DOS (for PBE see Fig. 8, for U=2 eV see Fig. 9, for U=4 eV see Fig. 10, and for U=6 eV see Fig. 11 there is a clear trend to be seen studying the local DOS. The larger the value of U the larger is the splitting between characteristic Fe peaks and the smaller the hybridization between Fe and O states as can be seen in particular in the energy range from -5 to -2 eV. There, the red curve (Fe states) is reduced when compared to the blue curve (O states). A particularly large splitting effect of Fe states is seen for the U=6 eV case: A very large majority spin peak occurs at about -8 eV (with almost no hybridization) whereas its minority spin counter part is found at 2 eV where it hybridizes with the unoccupied La f-states. In all cases apart from U=6 eV the system is metallic with a sizeable contribution of spin down states at the Fermi energy, whereas in the DOS for U=6 eV (Fig. 11) a very small gap can be seen in the DOS as shown by Fig. 11.

U (V)	E_0/atom (eV)	ΔE_0 (eV)	m_{Fe} (μ_B)	m_O (μ_B)	V_0	a (Å)
PBE	-8.021	0	2.58	0.07	11.52	3.86
2	-7.865	+0.156	3.30	0.10	11.82	3.90
4	-7.649	+0.372	4.20	0.19	12.31	3.95
6	-7.521	+0.500	4.38	0.27	12.32	3.95

Table 1: DFT results for the FM magnetic ordering with 5 atoms in the unit cell. Data refer to the equilibrium volume at which the total energy has a minimum. The table shows the total energy E_0/atom for PBE only and several U parameters, energy difference ΔE_0 with respect to the PBE result, local magnetic moments m_{atom} of Fe and O for FM $LaFeO_3$, equilibrium volume V_0 per atom and the cubic lattice parameter.

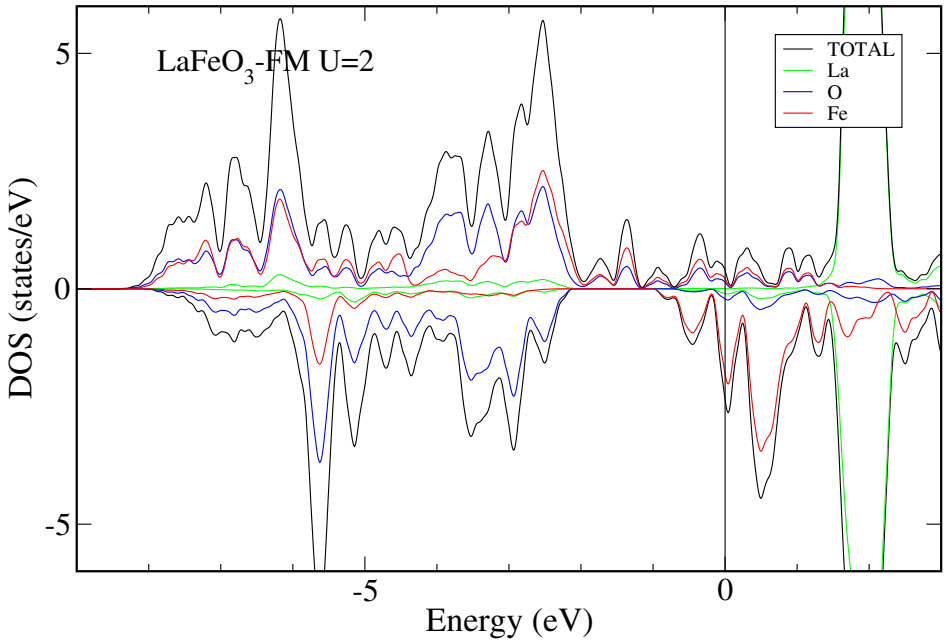

Figure 9: Total and local spin-split density of states (DOS) of FM $LaFeO_3$ due to FM ordering with U=2 eV. DOS of spin/up down states has positive/negative values.

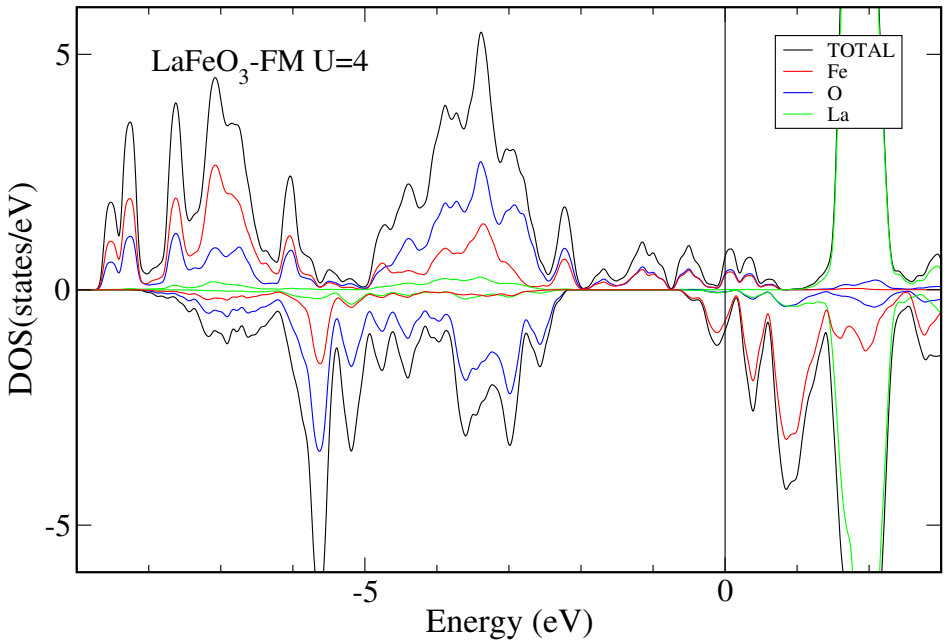

Figure 10: Total and local spin-split density of states of FM $LaFeO_3$ due to FM ordering with U= 4eV. DOS of spin/up down states has positive/negative values.

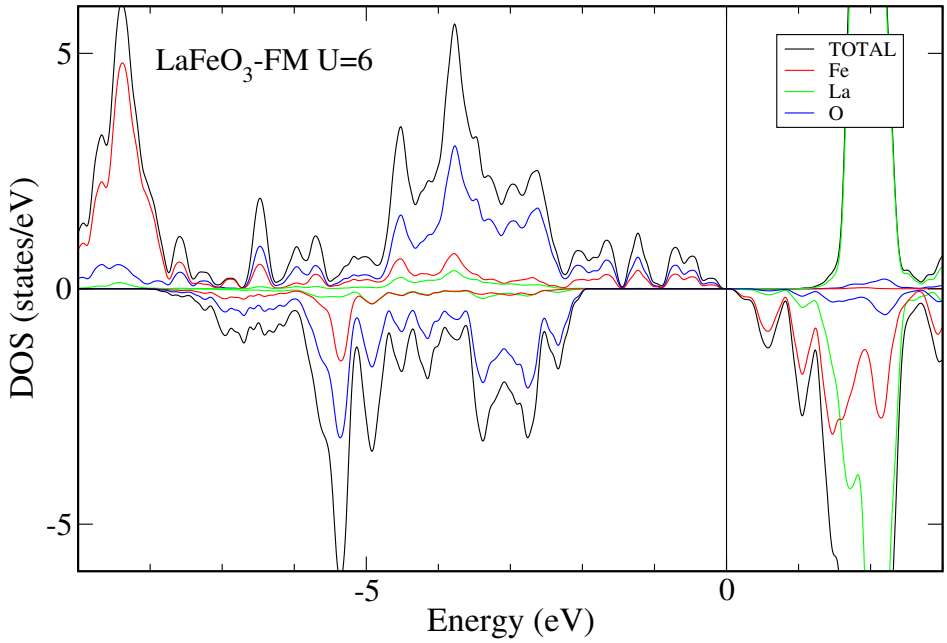

Figure 11: Total and local spin-split density of states of FM $LaFeO_3$ due to FM ordering with U= 6 eV. DOS of spin/up down states has positive/negative values.

6.2 A-type antiferromagnetic $La_2Fe_2O_6$

For describing the crystal structure of $LaFeO_3$ with layerwise A-type antiferromagnetic ordering the unit cell has to be doubled along the z-axis as compared to the FM case resulting in tetragonal unit cell with composition $La_2Fe_2O_6$. The calculations were performed with ISIF=3 and ISIF=2 (see VASP manuel) and the results compared. For the **k**-space integration a $8 \times 8 \times 4$ grid was chosen and other parameters kept same as for the 5 atoms unit cell (See Appendix 9.2) The Table 2 shows the equilibrium total energies per atom for A-type AFM as well as the local magnetic moment of Fe. In comparison with Table 1 it is found that for PBE and U=2 eV the FM ordering has lower total energy per atom as A-type AFM, and is therefore predicted to be stable. For larger values of U, U=4 and 6 eV the A-AFM structure becomes more stable, which is in agreement with the study of Koubský. In the DFT study of Sarma *et al.* [37] the experimentally observed crystal structure of $LaFeO_3$ was employed. Theses authors applied LAPW and LMTO-ASA methods with the LDA (or LSDA for spin polarized calculations) approximation and no U. In contrast to the present PBE results they found A-AFM more stable than FM. In the present work using a significantly more elaborate computational scheme (i.e. optimizing the geometrical parameters and using the GGA-PBE potential), the stability changes with increasing U.

Discussing the local magnetic moments as listed by Table 2 it should be noted that -because of symmetry- the local moments of O are exactly zero. Again, -as expected- with

increasing U and localization of the occupied Fe d-states the local moments increase reaching again some kind of saturation for U=6 eV. A similar bahviour is found for the volume per atom, as discussed for the FM case in the previous chapter. Concerning the c/a ratio with U=4 and 6 eV the c/a ratio is slightly smaller than 2 (rather close to the cubic case of c/a=2) in contrast to the results for PBE and U=2 eV. There, c/a is larger than 2 and the deviation from the cubic symmetry is mor significant.

U (eV)	E_0/atom (eV)	ΔE_0 (eV)	m_{Fe} (μ_B)	V_0 (Å^3)	c/a
PBE	-7.988	0	$\pm$ 2.62	11.56	2.064
2	-7.855	+0.133	$\pm$ 3.59	11.65	2.064
4	-7.675	+0.313	$\pm$ 4.16	12.28	1.997
6	-7.542	+0.446	$\pm$ 4.32	12.28	1.984

Table 2: DFT results for the A-AFM magnetic structure consisisting of 10 atoms in the unit cell. Data refer to the equilibrium volume at which the total energy has a minimum. The table presents the total energy E_0/atom for several Coulomb parameters U, energy difference ΔE_0 with respect to the PBE result, local magnetic moments of Fe, and the equilibrium volume V_0 per atom. Local moments of O are zero due to the antiferromagnetic symmetry.

Fig. 12 show the DOS of the PBE calculation. Because of symmetry the spin-up and -down DOS are the same, i.e. symmetric in the figure. The interest of this part of the calculations is to see the symmetrical up-spin and down-spin electrons in part from the usual hybridization feature as already discussed for the FM case there is a striking feature found in the DOS for A-AFM: at Fermi energy the DOS has a large peak arising from Fe d-states. This is quite in contrast to the FM DOS shown in Fig. 8, where E_F falls into a deep minimum of the DOS. Therefore, just inspecting both DOSes it becomes obvious that FM is mor stable than A-AFM. Indeed, checking the total energy per atom it turns out, that for FM the energy is 33 meV lower than for A-AFM.

The DOS features change very significantly when U=6 eV is used in the calculation as can be seen in Fig. 13. Again -very similar to the FM case- a very large splitting of the Fe main peaks occurs, but now the band widths are smaller and a gap has the chance to occur. This gap of about 0.6 eV agrees reasonably with the value of Koubský [30]. It should be noted that very small values of DOS are found just above and below the true gap, which cannot be resolved in the DOS.

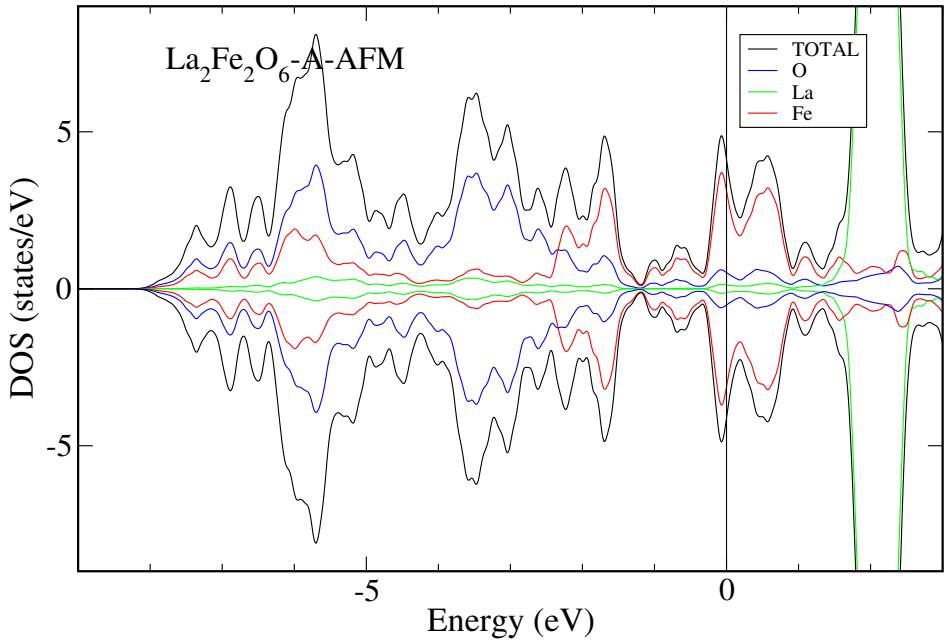

Figure 12: Total and local density of states of A-type antiferromagnetic $LaFeO_3$ in the 10-atom perovskite unite cell of the PBE calculation. Positive/negative values: spin up/down contributions. Fermi energy at E=0.

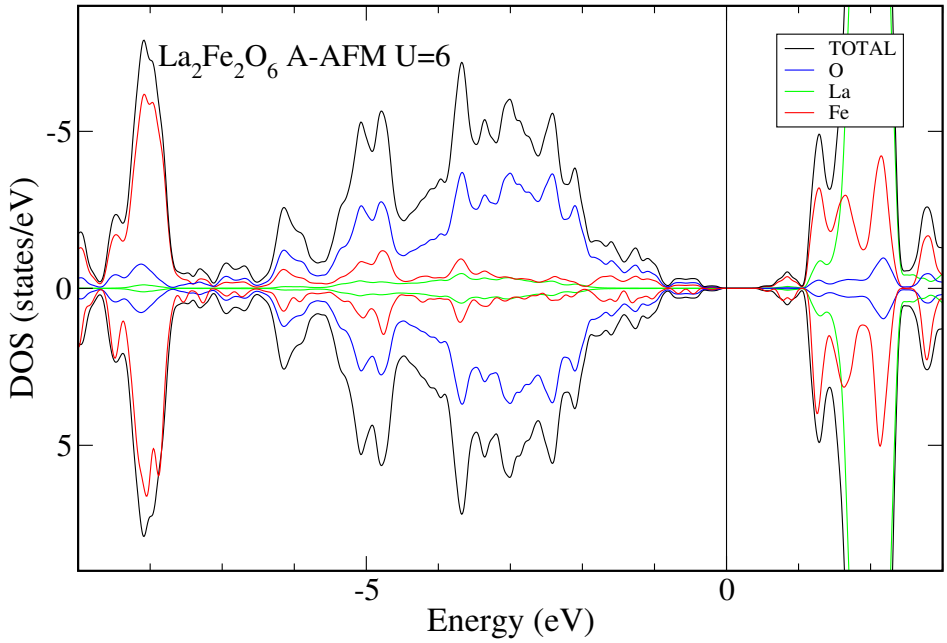

Figure 13: Local density of states of $LaFeO_3$ due to A-AFM as in Figure 12 but for U=6 eV.

6.3 $La_8Fe_8O_{24}$

In this section, the simple cubic unit cell containing 5 atoms was doubled in all three dimensions accomodating now 40 atoms. The enlargement is necessary in order to provide enough degrees of freedom for studying the most important antiferromagnetic structures such as the G-AFM structure as discussed above. Furthermore, such a large cell alows to introduce oxygen vacancies with a minimum concentration of 4% of the total oxygen composition. For the three magnetic orderings, FM, A-AFM and G-AFM VASP calculations were made within the GGA+U approach choosing U=6 eV and J=1 eV resulting in an effective Coulomb parameter of U-J=5 eV, as done in previous sections. Also the computational parameters were the same and **k**-point grid of $8 \times 8 \times 8$ points was used. All calculations are fully relaxed on the basis of ISIF=3 (full relaxation of all possible geometrical parameters: volume, cell shape and atomic positions) runs which were partially cross checked by ISIF=2 (only atomic positions relaxed) calculations. Table 3 summarizes some of the main results for the relaxed structures. From the column referring to ΔE one realizes that the G-AFM ordering is significantly more stable than A-AFM followed by the FM value, which is in accordance with experimental [31] (see also Table 5) and theoretical studies [30], [8], [15].

mag. phases	E_0/atom (eV)	ΔE/atom (eV)	m_{Fe} (μ_B)	V_0/atom (Å^3)
A-AFM	-7.542	+ 0.128	$\pm$4.32	12.28
FM	-7.521	+ 0.149	4.38	12.32
G-AFM	-7.670	0	$\pm$ 4.22	12.47

Table 3: VASP results for equilibrium properties of three magnetic structures of $La_8Fe_8O_{24}$ in terms of total energies and energy differences with respect to G-AFM, local magnetic moments m_{Fe} of Fe and equilibrium volume V_0 per atom.

According to Table 3 the local magnetic moments of Fe are large and rather similar for all three orderings as one would expect from the rather localized treatment of the d-orbitals. Concerning the equilibrium volumes, however, the G-AFM structure has a volume which is about 1.4% larger than the other two values. The 40 atom unit cell for the G-AFM structure can be reduced to a cell for half of the number of atoms resulting in an orthorhombic cell. The resulting lattice parameters are summarized in Table 4. The last column shows the results of the present study. The agreement with the experimental values is good, the values differ less than 1%. The experimental data are always slightly smaller than the values in the last column indicating that the DFT+U volume is smaller by about 3%. The results of another VASP study also applying GGA+U [8] (third column) are somewhere in between. In this study, which presumably used the same GGA+U procedure (LDATYPE=2 in the INCAR

file) an effective parameter of U-J=4.3 eV, which is slightly smaller than the value of 5 eV applied in the present study. It seems not plausible that such a small difference of the U parameters might be responsible for the difference. In particular so, when the results for the FM (Table 1 and A-AFM (Table 2) studies are considered, which yields the same volume for U=4 and 6 eV (or effective parameters of 3 and 5 eV). The difference in volume of the two VASP calculations might be due to the quality of the relaxation procedure. In the present case a rather high accuracy was demanded for the ISIF=3 calculation.

latt. param. (Å)	Exp. Ref. [31]	GGA+U [8]	GGA+U, present
a	5.553	5.572	5.584
b	5.563	5.627	5.642
c	7.862	7.901	7.919

Table 4: Orthorhombic lattice parameters of the G-AFM ordering.

	GGA+U, present	GGA+U	LDA+U	Exp.
m_{Fe} (μ_B)	4.22	4.2 [30], 4.2 [8]	4.1 [8], 4.06 [15]	4.6 [31]
E_{gap} (eV)	2.55	2.62 [30], 2.53 [8]	2.31 [8], 2.52 [15]	2.1 [32], 2.1 [33]

Table 5: G-AFM $LaFeO_3$: Comparison of electronic properties between different calculations and experiment: band gap E_{gap} and local magnetic moment of Fe.

Table 5 provides a comparison between different calculations and experimental data for some electronic properties. The local moments of about 4.2 μ_B agrees very well between the GGA+U calculations and even the LDA+U results. The value derived from experiment is significantly larger which might -at least partially- be attributed to the model which is used by the experimentalists to deduce the local moment from their measured data. It also should be kept in mind that in the calculations the local properties are defined within an atomic sphere, for which the radius has to be chosen. Since, however, the DFT+U treatment for larger U parameters strongly localize the 3d-functions it can be safely argued that local properties of Fe are then largely independent of the choice of the radius (assuming that it is in a reasonable range of values, such as the Wigner Seitz radius deduced from pure Fe).

The band gaps of the GGA+U calculations also agree very well with each other, being larger by about 20% than the experimental value. Again, one has to carefully check the way how this value is derived from the actual measured data. On the other hand one has to keep in mind that the choice of the U parameter influences the size of the band gap. Persumably, the choice of U=6 is somewhat to large in comparsion with the paper of [8], in which an effectice U=J of 4.3. eV was used, which in the present case is 5 eV.

The occurence of a gap has two reasons: the splitting of the Fe states between occupied and unoccupied states is very large (due to the large U=6 eV) and a simple electron counting rule assuming that both lanthanum and iron are in a 3+ ionic state. Referring to the most simple formula unit $LaFeO_3$ this would mean that 6 valence electrons are provided for the 3 oxygens, which end up in perfect O^{-2} states.

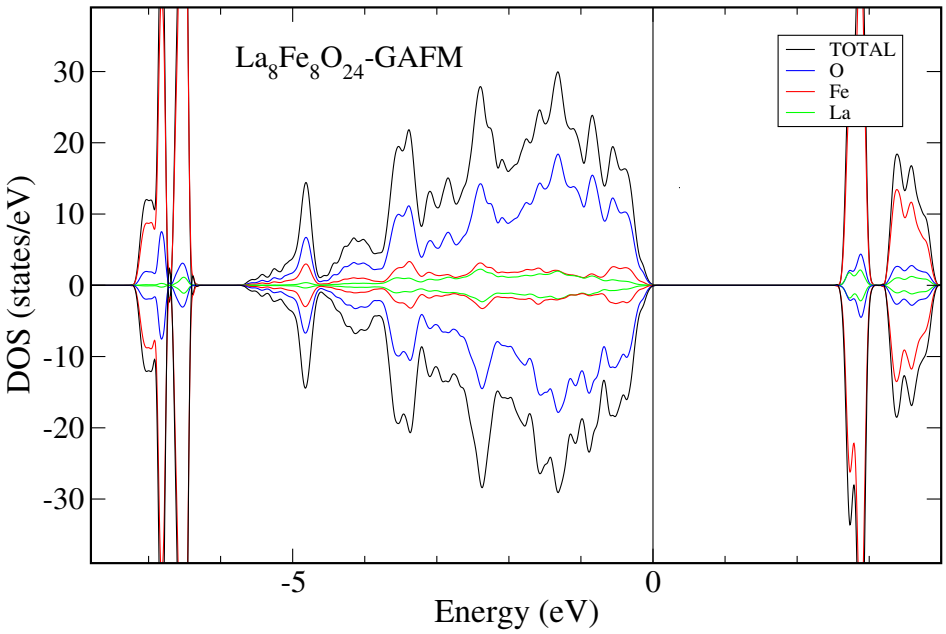

Figure 14: Total and Local density of states of $La_8Fe_8O_{24}$ with G-type antiferromagnetic ordering. VASP calculation was done with GGA+U potentials utilizing U=6 and J=1 eV.

Fig. 14 shows the symmetrically spin polarized of $La_8Fe_8O_{24}$ with a G-type antiferromagnetic ordering. This cell is twice as large as the smallest possible unit cell for this type of magnetic ordering. One notices the very large splitting of strongly localized iron states, which is enforced by the large U=6 eV parameter. The hybridization with O-s states (-7 – -6 eV) as well with the O-p states (-5.5 – 0 eV) is rather small due to the enforced strongly localized character of the Fe-d states. The splitting bteween the two main peaks of Fe is about 9 eV and the energy gap is 2.50 eV which agrees with the results of E. Carter *et al.* [8] and T. Koubský [30]. Previously, Wadata et al. [33], measured a gap of 2.1 eV with x-ray photoemission and absorption (XAS) and at this time compared with LDA+U (U_0= 2 eV) calculations [34], which failed to describe the gap character properly. The XAS spectrum is similar to the represent result in Figure 14, considering the energies of unoccupied d states and the band gap, but it gives different energy values for the occupied state of Fe. However, one should keep in mind that a comparison between DOSes derived from Kohn-Sham calculations with experimental spectra is ony qualitatively useful.

6.4 $Sr_8Fe_8O_{24}$

La has been replaced with Sr and the calculations were repeated in the same way as for the La compound. La was replaced by Sr and the calculations were repeated in the same way. Coming back to the simple ionic counting rule as introduced before for the G-AFM ordering of the La-compund it becomes obvious that the replacment of La^i+3 by Sr^{+2} must lead to a metallic character of the Sr-compound. There are not enough electrons to give each oxygen two additional electrons for its desired perfect O^{-2} ionization states. Therefore, for the G-AFM ordering Fermi energy must fall into the energy region of O-p states, as demonstrated by 15. Its metallic character has been already observed by x-ray photoemission and ultraviolet photoemission spectroscopy [35]. Tables 6 and 7 compare ground state properties of the present calculation with previous calculations and experiment as shown in Table 7 [36]. The measured cubic lattice parameter is reported as a=3.85 Å [35] which is about 2% smaller than the presntly calculated one of 3.92 Å for the FM and 3.94 Å for the G-AFM case. A calculation utilizing LDA+U [24] yielded smaller values of 3.97 and 3.80 Å for both magnetic phases. The overestimation of the experimental lattice parameter by GGA and the understimation by LDA is a typical volume effect of the respective approximations to the exchange-correlation functional. However one should also take into account that large values of U were applied which also lead to a volume expansion due to the magnetic pressure. By applying a simple model [35] and neutron scattering measurement [36] the magnetic moment of iron was measured as as 3.1 μ_B which is significantly smaller than the calculated values being larger than 3.9 μ_B. In Ref. [35] a rather complicated antiferromagnetic ordering was suggested (although based on a rather crude ligand field model) whereas the present calculation and Refs. [30, 24] predict G-AFM ferromagnetic ordering more stable by 50 meV per atom. This difference is rather significant and may raise some suspicion cencerning the validity of the experiment. Even more so because a large U was involved in all the calculations which should favour antiferromagntism. Nevertheless, FM is predicted by the calculations.

The DOSes as shown in Figs. 15 and 16 clearly reflect the argument given above about removing one valence electron per formula unit when compared to the corresponding La-compound. For the G-AFM case in Fig. 15 the Fermi energy moves away from the gap edge to the lower energy range because there are now 8 valence electrons less than for $La_8Fe_8O_{24}$, and now for the Sr-compound the G-AFM ordering becomes metallic. For the FM case a similar situation occurs with regards of the position of the Fermi energy and again a metallic character apperas. Above Fermi energy, however, an interesting feature occurs: within a gap of about 1.5 eV exclusively majority spin states occur. One might argue that adding a suitable number of valence electrons to the system (without changing the basic features of

	GGA+U, present	GGA+U, [30]	LDA+U (U=6eV, J=0.6) [24]
m_{Fe} (μ_B)	3.953	3.95	3.7
m_O (μ_B)	0.06		0.08
Δ E_0/atom (eV)	0	0	0
a (Å)	3.92	3.91	3.790
V_0 (Å ^{3})	12.00	12.00	10.89

Table 6: Physical properties of $SrFeO_3$ in the ferromagnetic ground state: Comparison with other theoretical studies and experiment. cal magnetic moments of Fe and O, cubic lattice parameter and equilibrium volume per atom. The FM state is lowest in energy when compared to other magnetic orderings and therefore the energy difference Δ E = 0.

	GGA+U,present	GGA+ U [30]	LDA+U [24]	Exp.
m_{Fe} (μ_B)	$\pm$ 3.96	3.96	3.64	3.1 $\pm$ 0.1
ΔE_0/atom (meV)	50	49	52	
a (Å)	3.94	3.94	3.80	.85
V_0 (Å ^{3})	12.24	12.23	10.97	11.41

Table 7: Physical properties of $SrFeO_3$ in the G-antiferromagnetic ground state: Comparison with other theoretical studies and experiment. average local magnetic moment of Fe, energy difference Δ E woth respect to FM, cubic lattice parameter and euqilibrium volume per atom.

the electronic structure at least near Fermi energy) would place the Fermi energy exactly in this half-metallic region, as just discussed, with exclusively majority spin states at Fermi energy. Indeed this happens when Sr is partially replaced by La, as elaborated in the next subsection.

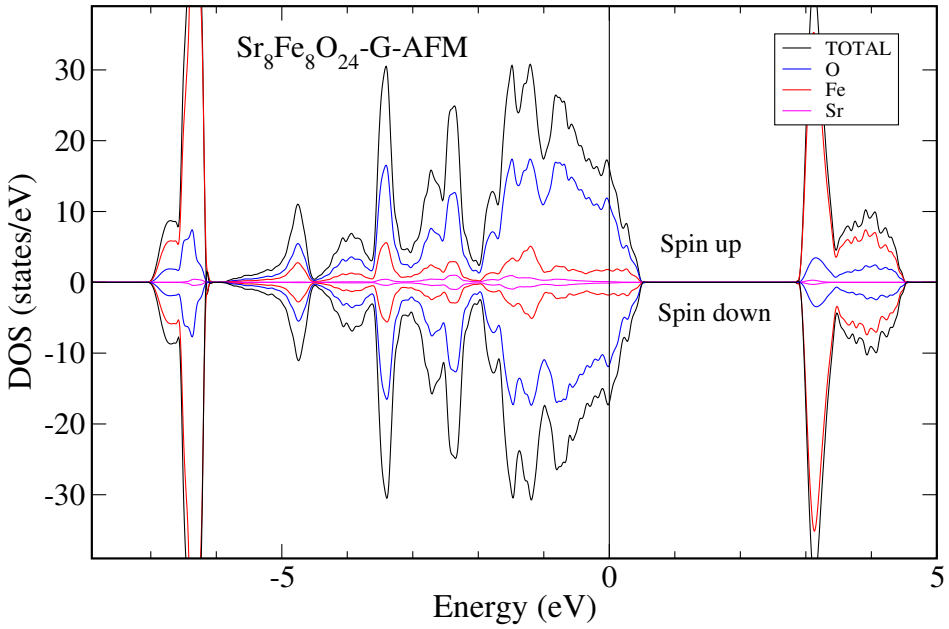

Figure 15: Total and local density of states of $Sr_8Fe_8O_{24}$ for the G-AFM magnetic ordering.

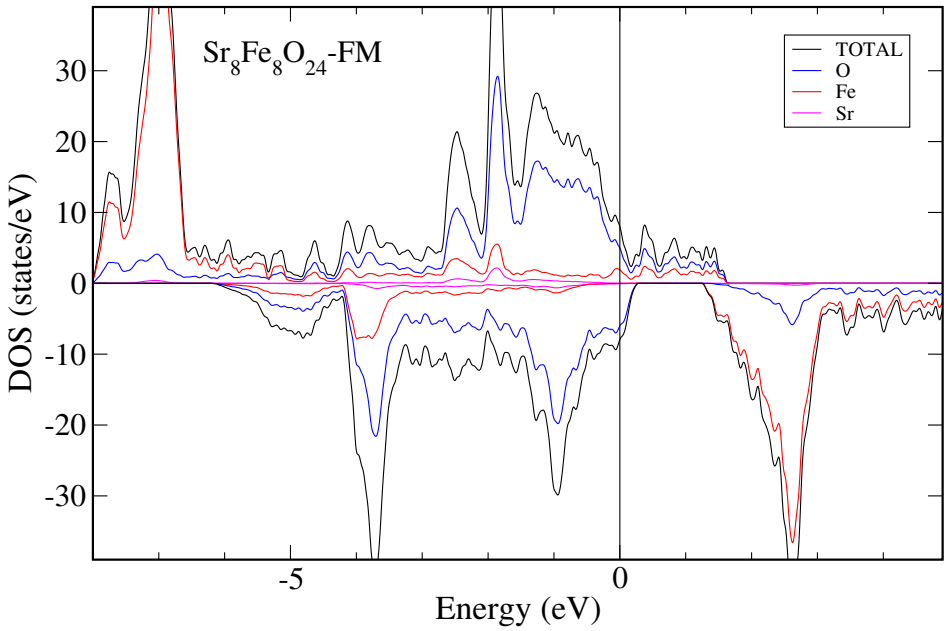

Figure 16: Total and local density of states of $Sr_8Fe_8O_{24}$ for the feroomagnetic ordering.

6.5 $Sr_4La_4Fe_8O_{24}$

The study on mixed La-Sr ferrates (LSF) in particular is very important in order to understand the experimentally claimed massive generation of oxygen vacancies. Therefore, the first major step is to investigate the thermodynamical stabilities, i.e. the ground state prop-

erties. The second step –far beyond the scope of the present study– would be the modelling of the oxygen transport, which is very favorable for interfaces and surfaces containing LSF. There has been a great deal of experimental and some theoretical research done on the LSF [8]. A major question is, how to model the LSF. Experimentally it is known, that a mixture of about 50% of La and Sr yields the most promising compounds (with respect to the oxygen vacancy concentration). Also DFT+U studies were done by Carter *et al.* [8] for this mixture resulting in rather low vacancy formation energies. This study focused on the small concentration range of vacancies. As will be elaborated in the next section in this work the focus is put on large concentrations. Based on the supercell of $La(Sr)_8Fe_8O_{24}$ a variety of possible distribution of 4 La and 4 Sr is possible. In order to make the present study feasible two distinctly different La-Sr structures were constructed according to Fig. 17: Structure 1 consists of La and Sr layers (layer-wise mixing) when viewed along one of the cartesian axes; Structure 2 which contains mixed layers of Sr and La with the condition that the distance between equal atoms is a maximum. For each of the two different mixed structures calculations were done for the FM as well as for the G-AFM ordering using the same computational parameters (U=6 and J=1 eV) as for the pure La- and Sr-compound. The main euqilibrium results are summarized in Table 9. Independent of the Sr-distribution the FM solutions are always more stable by more than 20 meV per atom. The FM ordering for Structure 2 is only slightly more stable than Structure 1 indicating that the specific distribution of Sr atoms might be of rather negligible influence on the thermodynamic stability of the compound. In all cases the volumes and subsequently the cubic lattice parameter are very similar. The fluctuations being less than 0.5% in volume. The average local magnetic moments of Fe in the FM spin ordering is larger by $0.1\mu_B$ than for the antiferromagnetic cases. Its size is larger than 4 μ_B indication that –within a simplified ionic picture– iron may be considered as Fe^{+3} with 5 parallel spins.

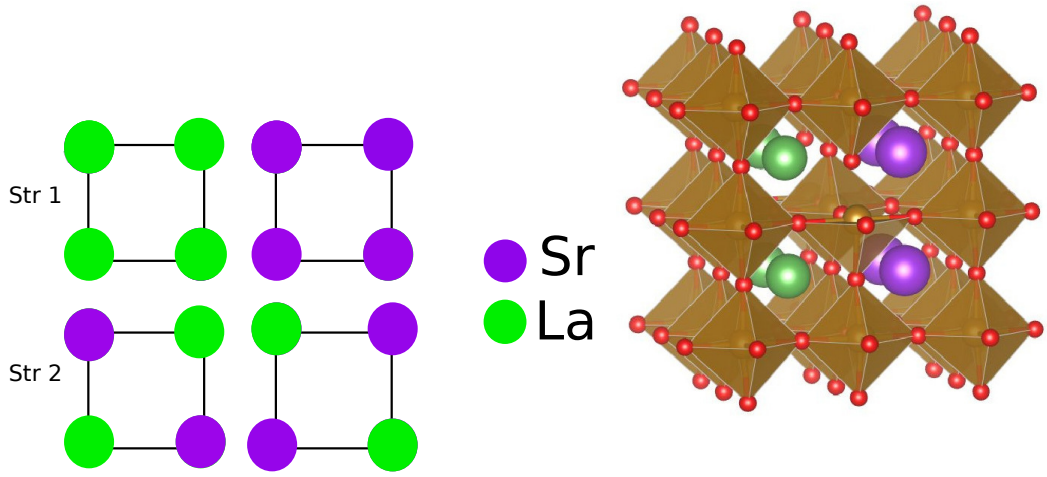

Figure 17: Sketch of the 2 distributions of La and Sr (Structure 1 and Structure 2) as studied here for $Sr_4La_4Fe_8O_{24}$.

structure	E/atom (eV),	ΔE/atom (meV)	m_{Fe} (μ_B)	V_0/atom (Å^3)	a(Å)
FM Str. 1	-7.014	1	4.13	12.14	3.93
FM Str. 2	-7.015	0	4.13	12.22	3.94
G-AFM Str. 1	-6.997	18	$\pm$ 4.03	12.22	3.93
G-AFM Str. 2	-7.004	11	$\pm$ 4.05	12.27	3.93

Table 8: VASP results of the GGA+U (U=6, J=1 eV) calculations for the two structures of $Sr_4La_4Fe_8O_{24}$ for both types of La-Sr distribution Structure 1 and 2 as described in the text. Results for ferromagnetic (FM) and G-type antiferromagnetic (G-AFM) orderings are shown. Equilibrium total energies and energy differences, average local magnetic moment of Fe equilibrium volume V_0 per atom, and lattice parameter a. Although no restrictions were imposed on the structure no significant deviation from the cubic structure was found.

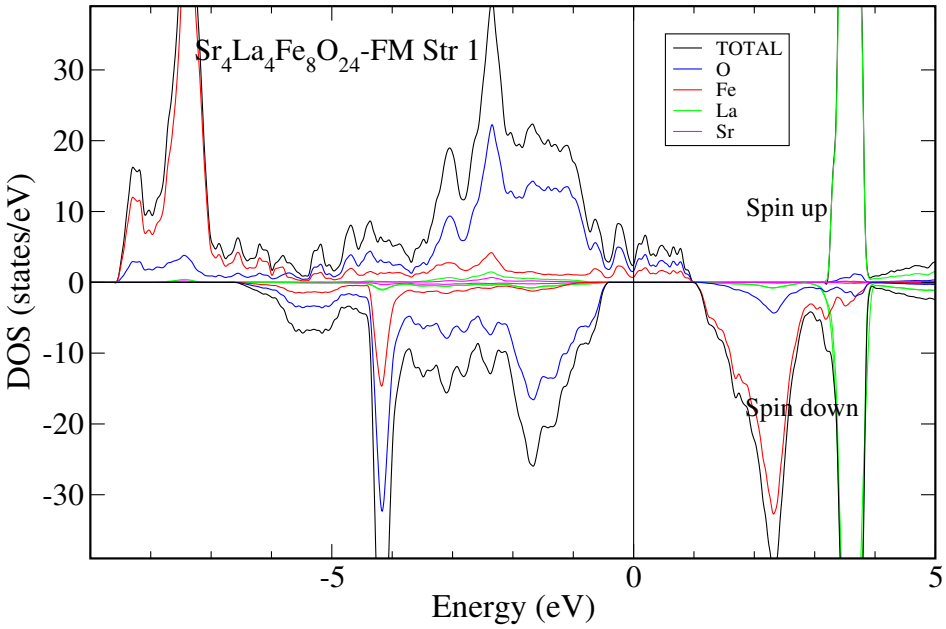

Figure 18: Total and local density of states of Str 1 of $Sr_4La_4Fe_8O_{24}$ with FM ordering.

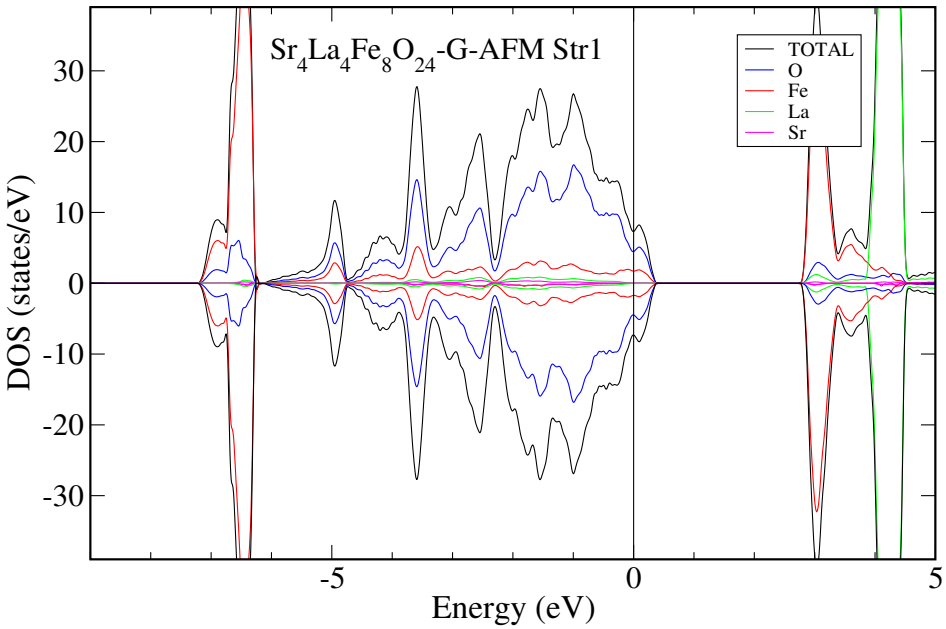

Figure 19: Total and local density of states of Str 1 of $Sr_4La_4Fe_8O_{24}$ with G-AFM ordering.

The DOSes in Figs. 18-21 reveal that the mixed compounds are all metallic. For G-AFM the DOS is very similar to the pure Sr-compound apart from the fact that Fermi energy lies close to the gap, because there are 4 electrons more in the mixed case. The FM cases are very

inteersting with respect to the position of E_F: it falls into an energy region with exclusively majority spin states indicating a possible usage of these compounds in spintronics. This situation does not occur for the pur Sr-compound because E_F lies below the gap of the minority spin states. The reason is clear: in the latter case there are 4 electrons less than for the mixed case. In the mixed case there is an interesting feature at about 1-1.5 eV. For Structure 1, a point of zero total DOS, whereas for Structure 2 a small gap already opens up.

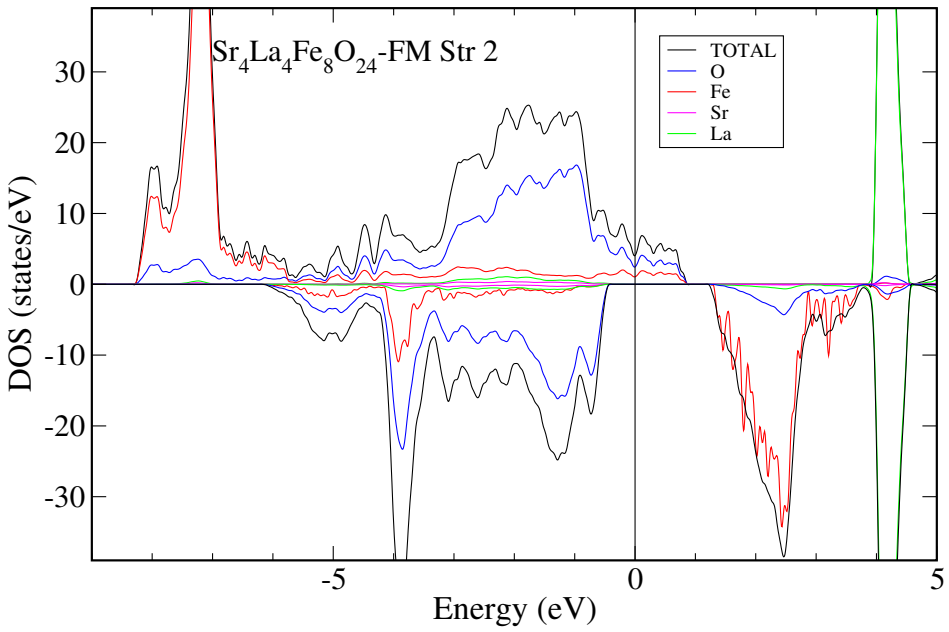

Figure 20: Total and local density of states of Str 2 of $Sr_4La_4Fe_8O_{24}$ with FM ordering.

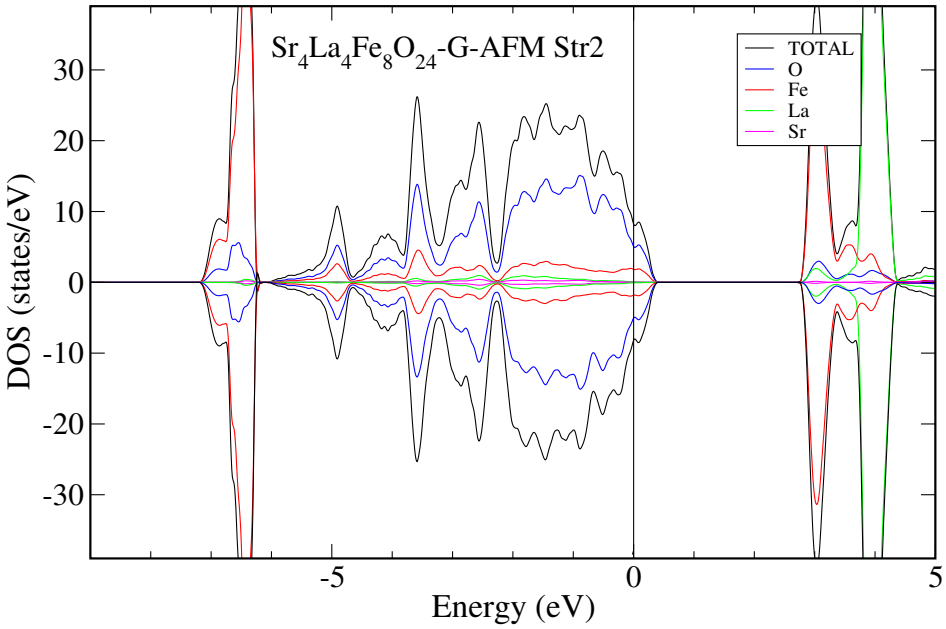

Figure 21: Total and local density of states of Str 2 of $Sr_4La_4Fe_8O_{24}$ with G-AFM ordering.

7 Oxygen Vacancies

The most important part of this study is the investigation of oxygen vacancies, because oxygen transport properties are crucial for the charge transport mechanism of SOFCs. Here, only the thermodynamic aspect of the formation energy of vacancies in a bulk material is considered. What would be further needed for a more realistic modeling of oxygen transport are activation barriers and the modeling of surfaces and interfaces. These latter points are far beyond the scope of a master thesis but will be the scope of the continuation of Special Research Branch FOXSI, of which this work is part of it. The actual work is done for single vacancies and pairs of them. The modeling is done by utilizing the unit cell $La_4Sr_4Fe_8O_{24}$ with 24 oxygens in it and removing one or two of them. Therefore the minimum concentration of vacancies per oxygen will be 4.2% which is quite large for isolated single point defects. However, it is well known from experiment that in the La-Sr ferrates a masive production of vacancies occur. This is also the reason, why pairs of vacancies are considered here, and –as it will be seen– are resulting in a thermodynamically rather stable system thus corroborating the actual observation by hard numbers. It should be noted, that such a massive occurence of vacancies cannot be treated by typical single point defects including temperature efects in terms of configurational entropy. Rather a concentration dependent treatment should be considered. For the definition of the vacancy formation energy the oxygen reference state was taken to be the free O_2 molecule which in the VASP calculation with periodic

boundary conditions was placed into a large box. The equilibrium results in terms of total energy and bond length could then be checked as a function of the box size. It should be noted, that O_2 must be calculated ferromagnetically because of the unfilled shells, the spin polarisation adds a considerable amount of bonding energy. Within PBE the total energy for the gound state of O_2 amounted to -9.782 eV. By that the thermodynamical reference state is the perfect compound and a free O_2 molecule. Now, the vacancy formation energy can be defined as

$$\Delta \mathrm{E}_{form}^{\text{O-vac}} = \left(\mathrm{E}_{hole}^{tot} + \frac{1}{2} \mathrm{E}_{\mathrm{O}_2}^{tot}(-9.782eV) \right) - \mathrm{E}_{perfect}^{tot} \tag{9}$$

for a single vacancy and

$$\Delta \mathrm{E}_{form}^{\text{O-vac}} = \left(\mathrm{E}_{hole}^{tot} + \mathrm{E}_{\mathrm{O}_2}^{tot}(-9.782eV) \right) - \mathrm{E}_{perfect}^{tot} \tag{10}$$

for a pair of missing oxygens.

In the calculations all structural parameters are relaxed by choosing the ISIF=3 option. All other numerical parameters are kept the same thus garanteeing a direct comparison of the VASP results.

The single oxygen vacancies were investigated for each case, namely for pure La and Sr compounds, mixed La-Sr compounds and different magnetic orderings. Pairs of oxygen vacancies were studied only for the Sr-La mixed cases (see Fig. 17), which is the most interesting one. For an exhaustive and complete vacancy study one would have to treat all possible different atomic configurations. Already for mixing La and Sr with even at equal proportions would require more than two cases and considering vacancies the number of possibilities is becoming much larger in particular for the G-AFM ordering and for pairs of vacancies. Nevertheless, by the selected procedures in this work the results obtained here are should be fairly representative for a complete investigation. Furthermore, the scattering of results due to different atomic configurations for the same magnetic ordering and composition is reasonably small, so that the major findings are not affected.

For each DFT+U (U=6, J=1) calculations, the 40 atoms supercell for each in their previously found most stable orderings were taken. The vacancy formation energies were calculated removing an oxygen from each 24 possible oxygen sites. For FM $SrFeO_3$, due to the symmetry, only one oxygen site was considered. For G-AFM $LaFeO_3$, calculations were done for 10 sites for the La-Sr mixture STRUC1 and for all 24 sites for STRUC2, which is the more stable one in the perfect case. For the double vacancies two cases for each structure and magnetic configuration were considered: 1) vacancies as nearest neighbours and 2) vacancies with the largest distance betwenn the original O-sites. The nearest-neighbour tables were investigated by using the DFT code flair [39] as shown in the Appendix 9.5,

7.1 $La_8Fe_8O_{23}$ in G-AFM ordering

For G-AFM ordering of $La_8Fe_8O_{24}$, the oxygen vacancies were created for 10 oxygen sites (see Appendix 9.4). The oxygen energy formation energies are calculated for each sites and the average is taken as written in Table 9, which shows that the energy cost to create one vacancy is very large. Nevertheless, the defect compound is still insulating as demonstrated by the DOS in Fig. 22. In comparison to the pure compound Fe-like peaks just below Fermi energy in the spin-up and down DOS occur. These structures split off from the main Fe-peaks because the ionization of Fe^{3+} is partially reduced because one oxygen is missing and two valence electrons are now available to be distributed in the system. Because of this splitting-off the gap is reduced. Clearly, the ionization of Fe is reduced as can also be send from the local magnetic moments: now the Fe around the vacancy have a significantly smaller moment of 3.70 μ_B because some of the originally empty minority-spin states are now filled. 10 possible oxygen sites in the supercell. A further unusual effect is the increase of volume when one oxygen is removed. In a simple ionic picture this might be understood in terms of the reduced attractive Coulomb interaction between the iron and oxygen atoms. Again it should be emphasized that the rather expressed ionic character of the ion atoms is due to the large value of U-J=5 eV.

The volume of the cell is getting increased by creating a hole. The local magnetic moment of iron is also giving slightly altering results, as it is shown in the Table 9. The band gap decreases from 2.5 eV to 1.3 eV, shown in Fig. 22. As comparison to the perfect structure Fig. 14, below the Fermi level, unsymmetrical spin polarization appear and huge iron state peak arises around -1 eV which also shows the electrons can easily move above fermi level, therefore the less stability of the system. However, the compound keeps its antiferromagnetic character.

	$\Delta E_{form}^{\text{O-vac}}$ (eV)	E_{gap} (eV)	m_{Fe} (μ_B)
Perfect Str.	0	2.5 eV	4.22
Single Vacancy	+4.193	1.3 eV	3.70-4.22

Table 9: Single oxygen vacancy properties for G-AFM $LaFeO_3$, vacancy formation energy $\Delta E_{form}^{\text{O-vac}}$ averaged over 10 sites, gap size E_{gap} and local magnetic moments of Fe.

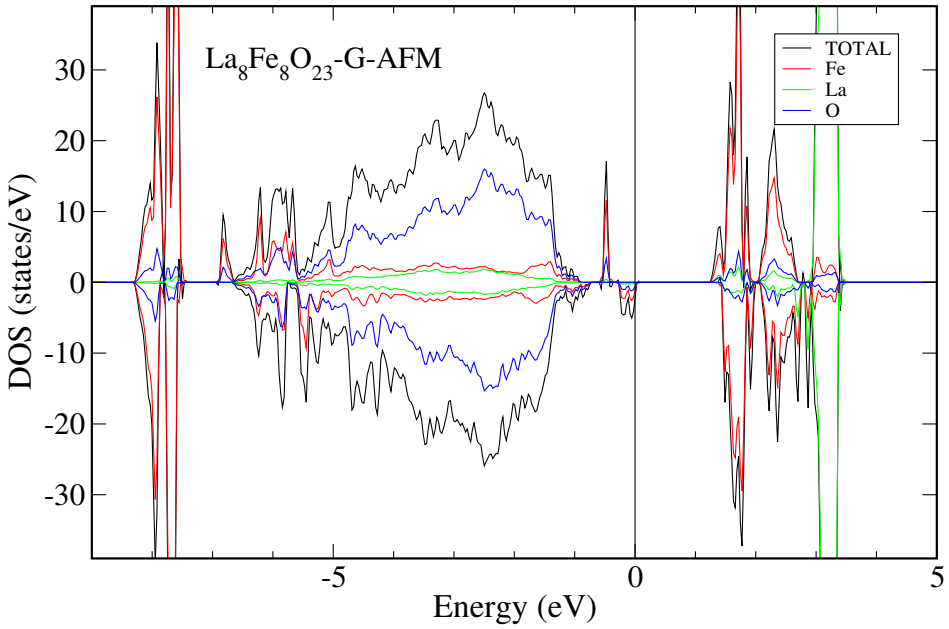

Figure 22: Total and local density of states of G-AFM $La_8Fe_8O_{23}$. The vacancy is created at the O_{18} position.

7.2 $Sr_8Fe_8O_{23}$ in FM ordering

As mentioned already due to symmetry (i.e. all Fe atoms are symmetrically equivalent) only one vacancy position needs to be considered for the FM ordered compound when studying single vacancies. Strikingly, the formation energy becomes very low as listed in Table 10. The magnetic moments of Fig. 23 the compound is metallic and the DOS does not change significantly when compared to the perfect case or the La-Sr mixed compound. Basically Fermi energy is just shifted according to the change in number of valence electrons.

	$\Delta E_{form}^{\text{O-vac}}$ (eV)	m_{Fe} (μ_B)
FM	0	3.98
Single Vacancy	+0.30	3.85-4.07-3.98

Table 10: Single oxygen vacancy properties of $Sr_8Fe_8O_{23}$. Formation energy $\Delta E_{form}^{\text{O-vac}}$ (eV) and local magnetic moment of iron.

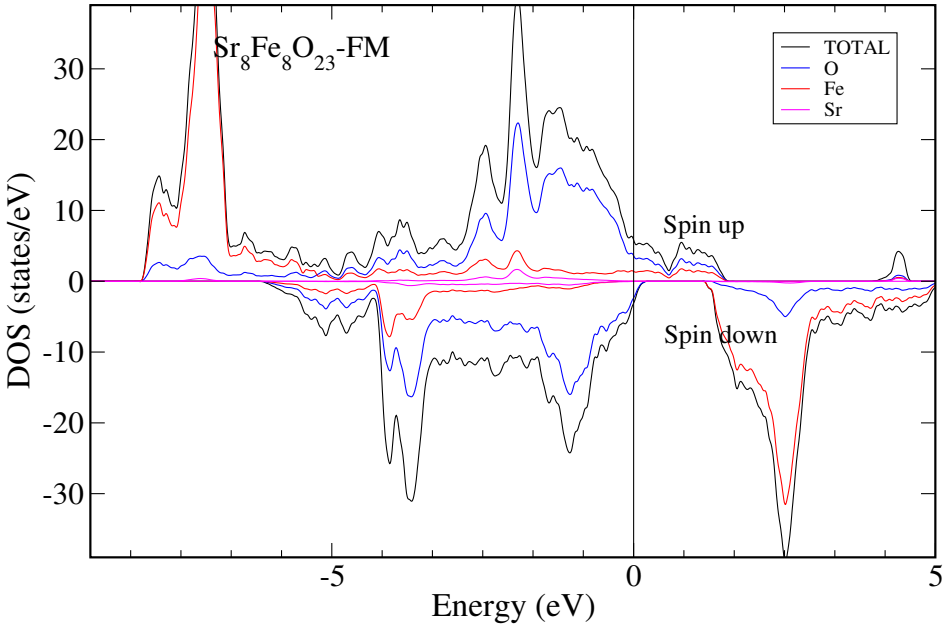

Figure 23: Total and local density of states of $Sr_8Fe_8O_{23}$ in FM ordering.

7.3 Single and pairwise oxygen vacancies in the mixed compounds $Sr_4La_4Fe_8O_{24-x}$ with x=1,2

7.3.1 $Sr_4La_4Fe_8O_{24-x}$ in G-AFM ordering and STRUC1 La-Sr distribution

Table 11 lists some results of the single and double vacancy calculation. Very strikingly, the energy of formation for the single vacancy (averaged over three sites) is negative which would indicate that the perfect compound would decay into the bulk compound with a vacncy plus a free oxygen molecule. It should however be noted, that this is only an information about the thermodynamical ground states, and there might be a sizeable activation barrier between them. Very noticeable are also the finding about the vacancy pairs. Clearly, the case for neares-neighbour vacancies is preferred in comparison to the case in which the two vacancies are further apart. Concerning the local moments there is also a significant difference between the single and double vacancies: whereas for the single vanacy the moment fluctuates significantly similar to the pure La-compound, it is rather constant for the pairs. This feature is again simply explained by a simple ionic model: The half-half mixture of Sr and La together with Fe^{3+} provides exactly the right number of valence electrons for the 22 O ions with charge -2. This cannot be achieved for single oxygen vacancy or 23 O atoms, and the ionicity of Fe fluctuates between 2+ (near the vacancy) and 3+.

This feature of ionicity is also expressed by the DOSes. The single vacancy case in Fig. 24 shows that the Fermi energy is placed below the gap edge separating a region of rather

low DOS from the rest. The system is metallic in distinct contrast to the case for vacancy pairs as shown in Fig. 25 and 26 for hich a large gap of about ≈ 2 eV occurs. Interestingly, for the vacancy cluster in Fig. 26 the DOS becomes slightly unsymmetric with respect to spin polarization.

G-AFM STR 1.	$\Delta E^{\text{O-vac}}_{form}$ (eV)	m_{Fe} (μ_B)
Perfect	0	$\pm$ 4.03
Single Vacancy	-0.628	$\pm$3.60 / $\pm$4.20
Double Vacancy short dist.	-0.414	$\pm$ 4.20
Double Vacancy long dist.	+0.090	$\pm$ 4.20

Table 11: Single and pairwise oxygen vacancies properties of $Sr_4La_4Fe_8O_{24-x}$ with G-AFM ordering in the STRUC1 mixing of La and Sr. Average quantities wherever needed. Formation energy per vacancy $\Delta E^{\text{O-vac}}_{form}$ for and average local magnetic moment of Fe.

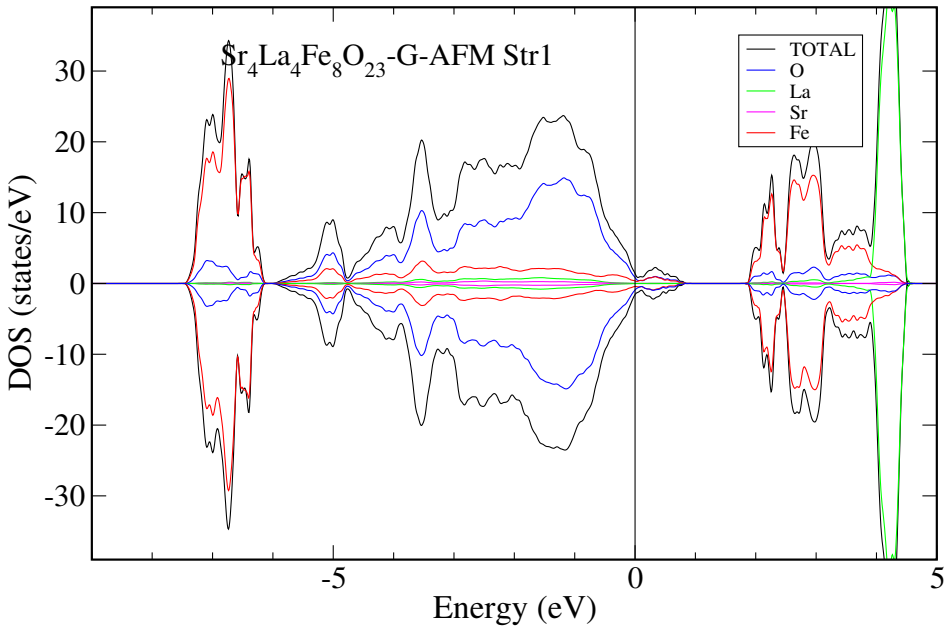

Figure 24: Total and local density of states of the single vacancy structure $Sr_4La_4FeO_{23}$ in the G-AFM ordering and the STRUC1 La-Sr distribution. Vacancy site: O18.

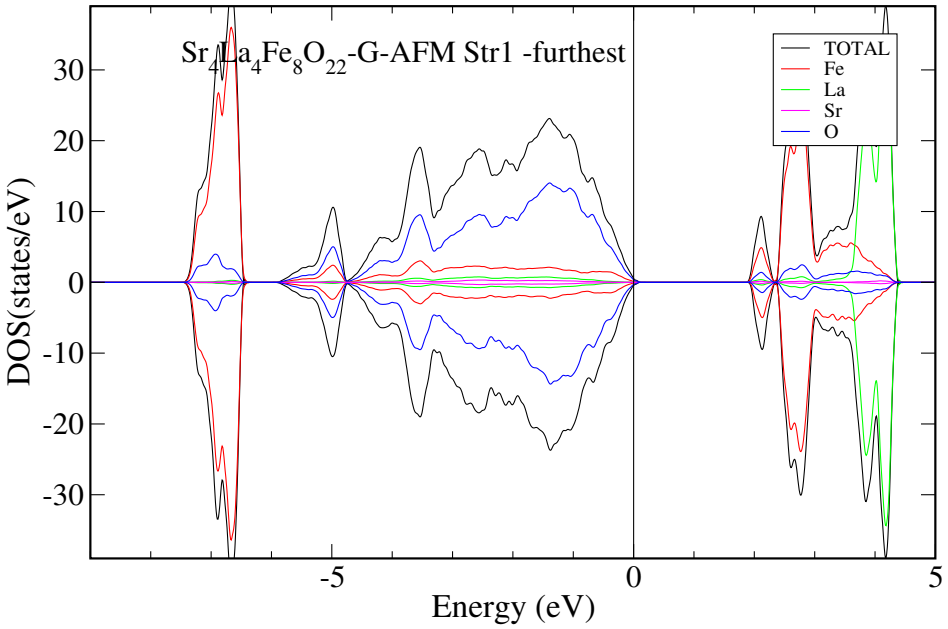

Figure 25: Total and local density of states of the vacancy pair compound $Sr_4La_4FeO_{22}$ in the G-AFM ordering and STRUC1 distribution. Long distance between the vacancy pair.

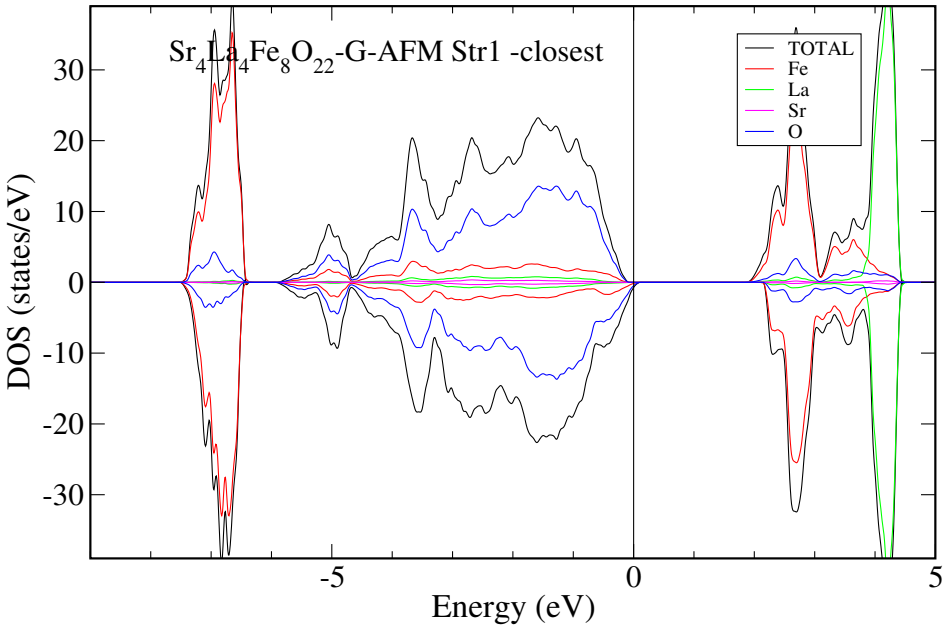

Figure 26: Total and local density of states of the vacancy pair compound $Sr_4La_4FeO_{22}$ in the G-AFM ordering and STRUC1 distribution. Shortest distance between the vacancy pair.

Some tests were made for a different set of vacancy sites but all the basic features including the DOSes remain rather unchanged.

7.3.2 $Sr_4La_4Fe_8O_{24-x}$ in G-AFM ordering and STRUC2 La-Sr distribution

Because the STRUC2 is slightly more stable than STRUC1, Table 12, all possible 24 oxygen sites (See Appendix 9.7) were considered for the single vacancy study. In Table 12 all values are therefore averaged. There is no significant difference to the study with STRUC1. In particular the formation energies are also low and even negative for the single vacancy. Converning the pair vacancies the difference between most far away and closest vacancy pair distances is less significant. Presumably other distributions might lead to similar results as for STRUC1. An exhaustive complete study seems to be prohibitively costly regarding all possible distributions. Nevertheless, in all studied cases the formation energies are very low. The behaviour of the local moments is very similar to STRUC1, showing the 2+ and 3+ ionicity fluctutation for the single vacancy case and the constant value for the vacancy pairs. The DOSes look very similar to STRUC1, but interestingly the small asymmetry with respect to spin-polarisation is now observed in both cases of pairwise vacancies.

G-AFM STR 2	$\Delta E_{form}^{\text{O-vac}}$ (eV)	m_{Fe} (μ_B)
Perfect	0	$\pm$ 4.05
Single Vacancy	-0.026	$\pm$ 3.60 - $\pm$ 4.22
Double Vacancy short dist.	+0.189	$\pm$ 4.18
Double Vacancy long dist.	+0.124	$\pm$ 4.18

Table 12: Single and pairwise oxygen vacancies properties of $Sr_4La_4Fe_8O_{24-x}$ with G-AFM ordering in the STRUC2 mixing of La and Sr. Average quantities wherever needed. Formation energy per vacancy $\Delta E_{form}^{\text{O-vac}}$ for and average local magnetic moment of Fe.

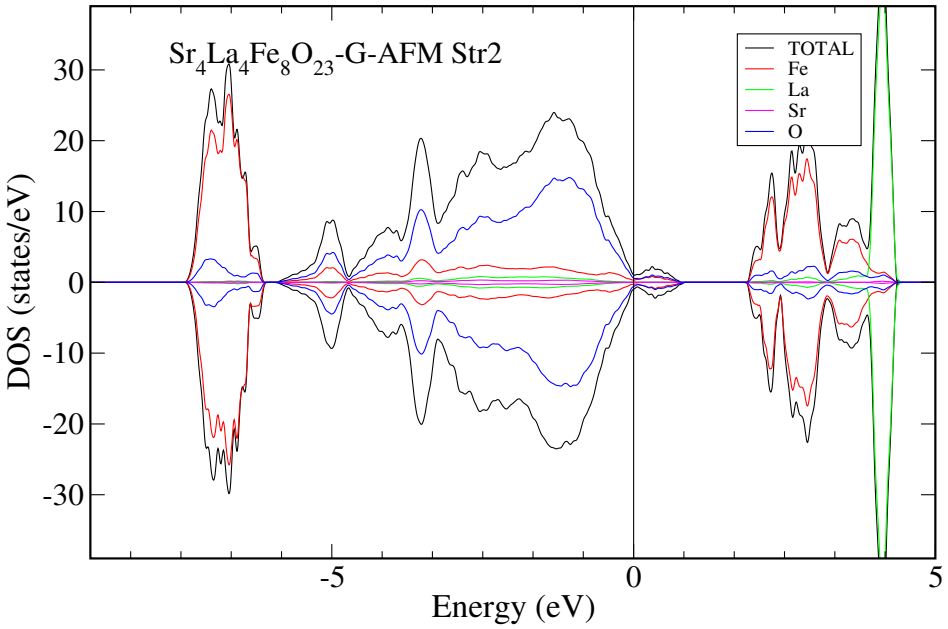

Figure 27: Total and local density of states of the single vacancy structure $Sr_4La_4FeO_{23}$ in the G-AFM ordering and the STRUC2 La-Sr distribution. Vacancy site: O18.

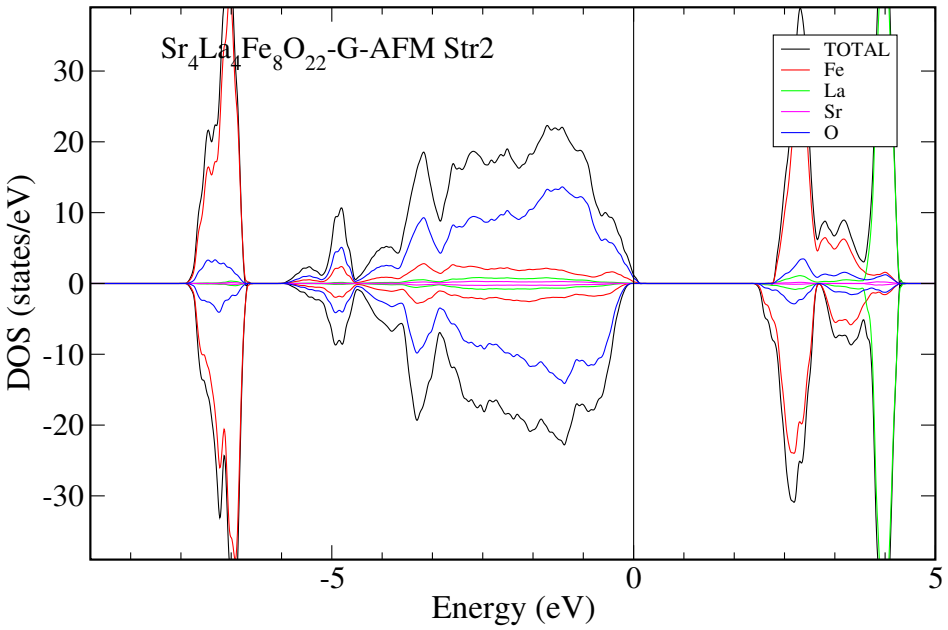

Figure 28: Total and local density of states of the vacancy pair compound $Sr_4La_4FeO_{22}$ in the G-AFM ordering and STRUC2 distribution. Shortest distance between the vacancy pair.

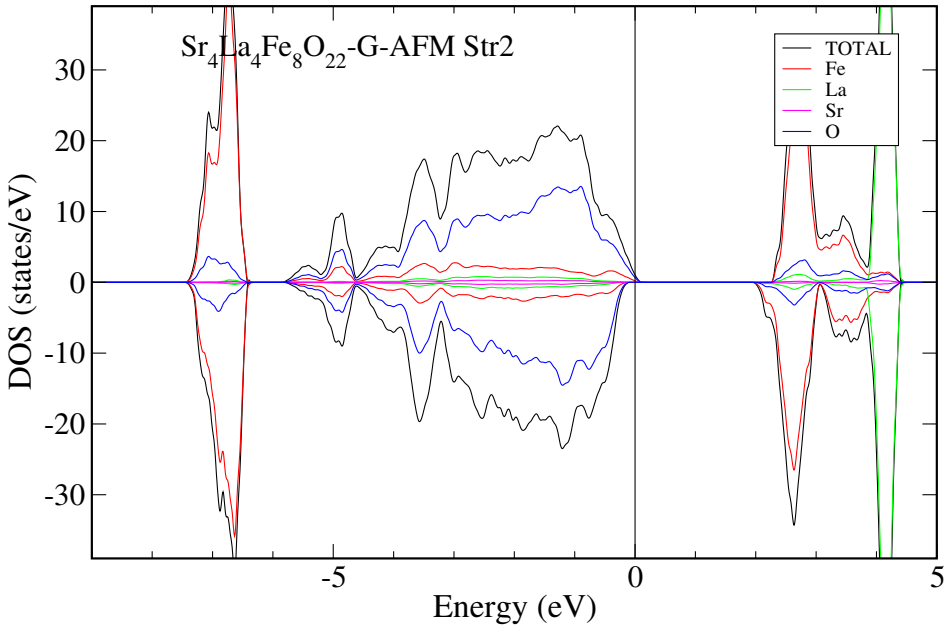

Figure 29: Total and local density of states of the vacancy pair compound $Sr_4La_4FeO_{22}$ in the G-AFM ordering and STRUC2 distribution. Longest distance between the vacancy pair.

7.3.3 $Sr_4La_4Fe_8O_{24-x}$ in FM ordering and STRUC1 La-Sr distribution

The vacancy properties for the FM case are different. Although the perfect FM structure is more stable than G-AFM the situation changes when vacancies are created. According to Table 13 the energy cost per vacancy are significantly larger than for G-AFM whereas the magnetic moments remain rather constant in all cases. Clearly the ionic character of Fe in the FM case seems to be more uniform.

FM STR. 1	$\Delta E_{form}^{O\text{-vac}}$ (eV)	m_{Fe} (μ_B)
Perfect	0	4.13
Single Vacancy	+0.819	4.23
Double Vacancy short dist	+0.997	4.32
Double Vacancy long dist	+1.209±	4.32

Table 13: Single and pairwise oxygen vacancies properties of $Sr_4La_4Fe_8O_{24-x}$ with FM ordering in the STRUC1 mixing of La and Sr. Average quantities wherever needed. Formation energy per vacancy $\Delta E_{form}^{O\text{-vac}}$ for and average local magnetic moment of Fe.

The single vacancy DOS for the FM case and STRUC1 looks very similar to the perfect case. Again, Fermi enegy falls into states of 100% spin polarized character. Agap of about

0.3 eV occurs between unoccupied states half an eV above Fermi energy. The single vacancy system is metallic.

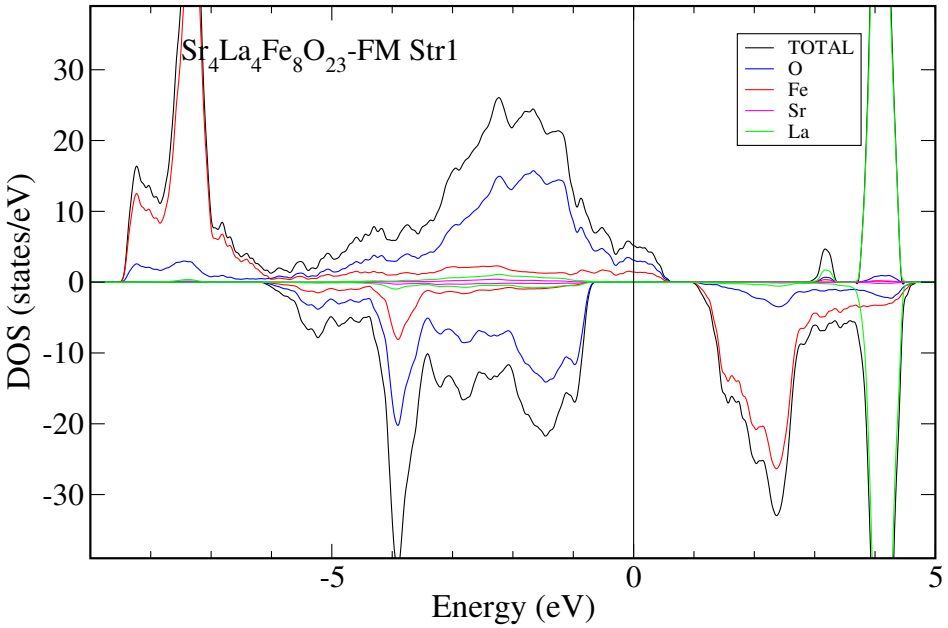

Figure 30: Total and local density of states of the single vacancy structure $Sr_4La_4FeO_{23}$ in the FM ordering and the STRUC1 La-Sr distribution.

Discussing the vacancy pairs for FM and STRUC1 a striking observation is made in both cases (i.e. shortest and longest distance of the vacancy pair): Fermi energy is now at the gap with sizes of about 0.3 eV. In this case the system is one of the rare cases of an insulating (or semiconducting) ferromagnet. The crucial occurence of the gap is due to the large U-J=5 eV value. Switching of the U,J parameters would lead to a breakdown of the gap and Fermi energy falls into a large value of the minority spin DOS, as shown by Fig. 35.

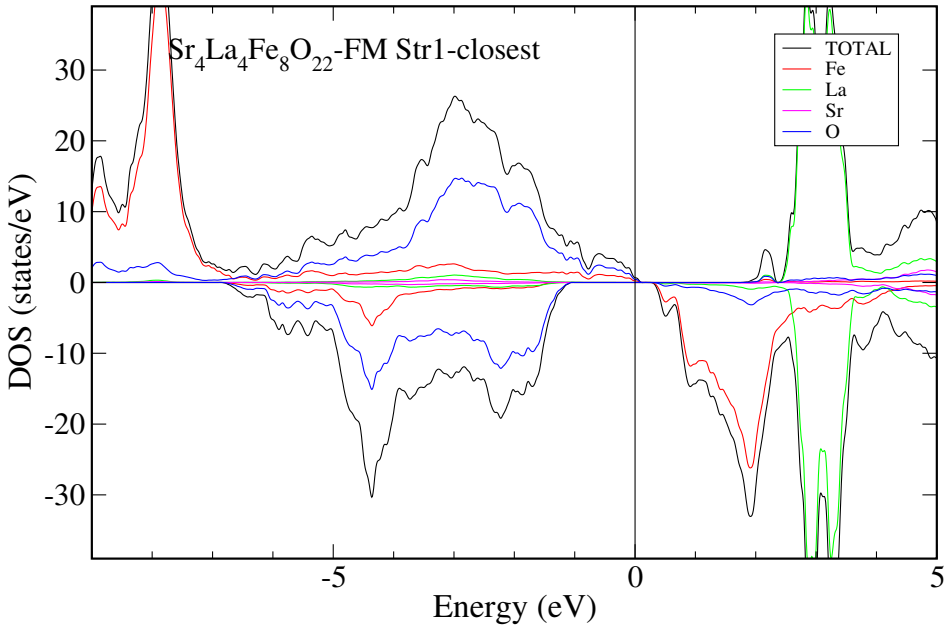

Figure 31: Total and local density of states of the vacancy pair compound $Sr_4La_4FeO_{22}$ in the FM ordering and STRUC1 distribution. Shortest distance between the vacancy pair.

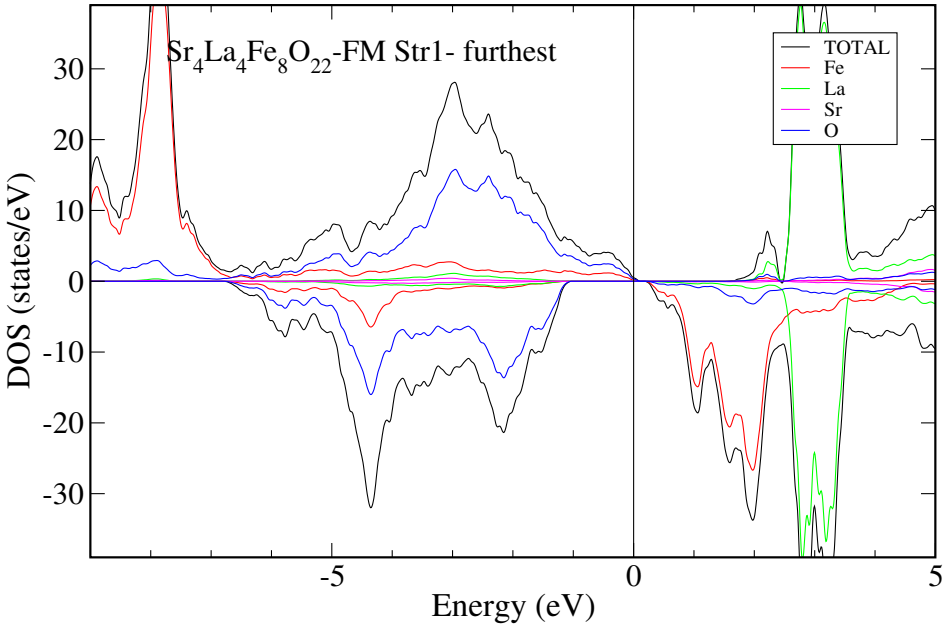

Figure 32: Total and local density of states of the vacancy pair compound $Sr_4La_4FeO_{22}$ in the FM ordering and STRUC1 distribution. Longest distance between the vacancy pair.

7.3.4 $Sr_4La_4Fe_8O_{24-x}$ in FM ordering and STRUC2 La-Sr distribution

In comparison with the STRUC1 La-Sr distribution in the previus subsection nothing changes for the second set of FM calculations. Therefore, no further discussion is necessary.

FM STR. 2	$\Delta E_{form}^{O\text{-vac}}$ (eV)	m_{Fe} (μ_B)
Perfect	0	4.13
Single Vacancy	+1.086	4.23
Double Vacancy short dist	+1.329	4.32
Double Vacancy long dist	+1.523	4.299

Table 14: Single and pairwise oxygen vacancies properties of $Sr_4La_4Fe_8O_{24-x}$ with FM ordering in the STRUC2 mixing of La and Sr. Average quantities wherever needed. Formation energy per vacancy $\Delta E_{form}^{O\text{-vac}}$ for and average local magnetic moment of Fe.

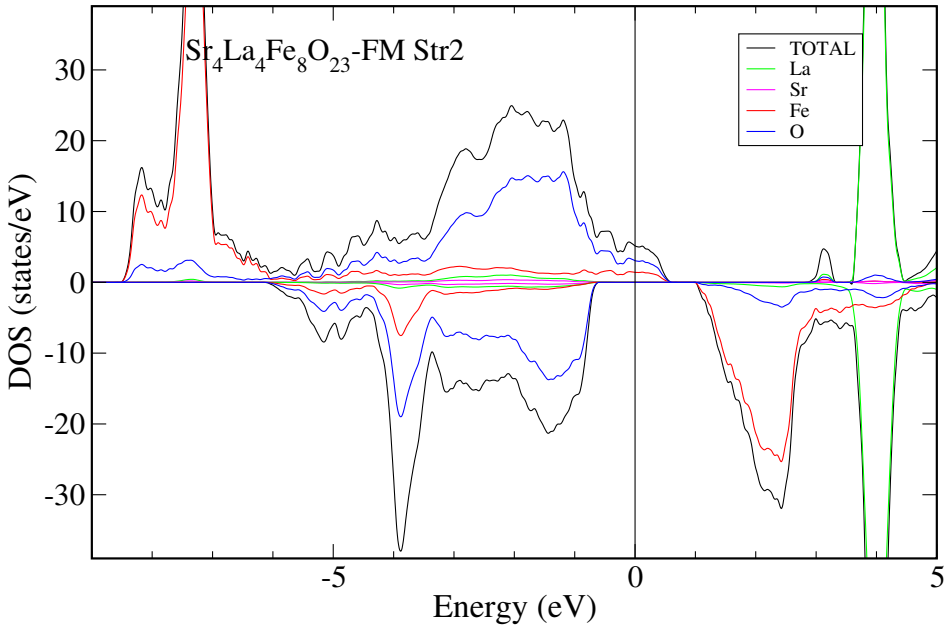

Figure 33: Total and local density of states of the single vacancy structure $Sr_4La_4FeO_{23}$ in the FM ordering and the STRUC2 La-Sr distribution.

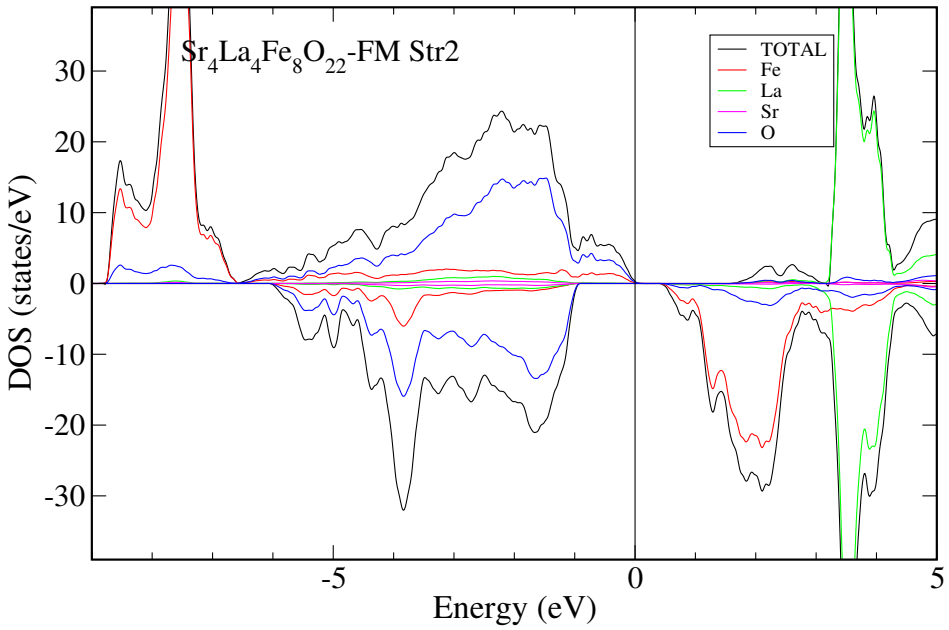

Figure 34: Total and local density of states of the vacancy pair compound $Sr_4La_4FeO_{22}$ in the FM ordering and STRUC2 distribution. Longest distance between the vacancy pair.

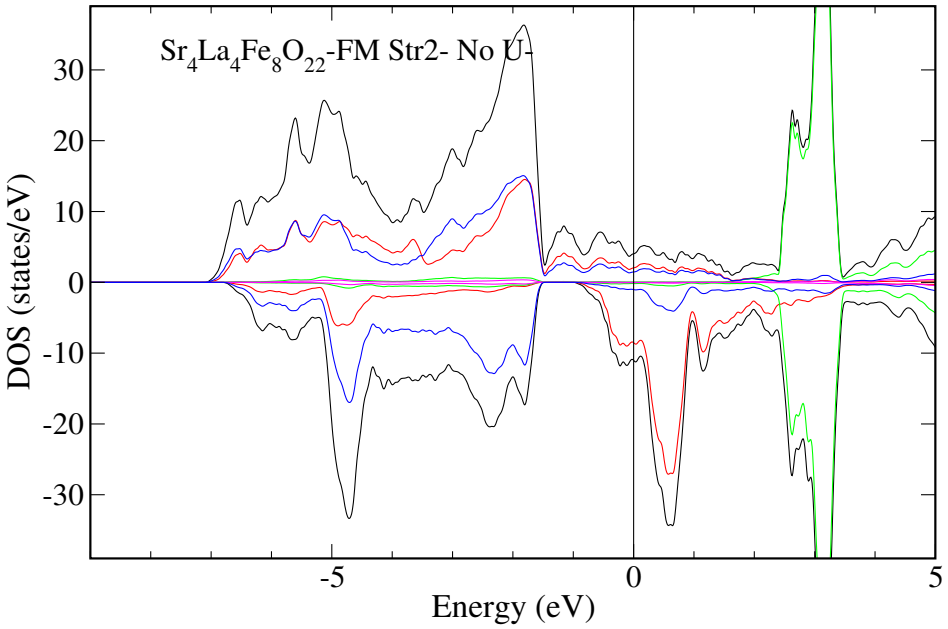

Figure 35: Total and local density of states of $Sr_4La_4Fe_8O_{22}$ with FM ordering and STRUC1 La-Sr distribution. Standard PBE calculation without any U, J parameters.

7.4 Summary of vacancy study

A striking feature of vacancy formation is the observation that with increasing number of vacancies also the volume per atom increases, which seems to indicated to the strongly ionic character of the bonding. Thinking in terms of overlapping wavefunction the atoms should rather move closer together. The same holds if atoms would be just hard spheres.

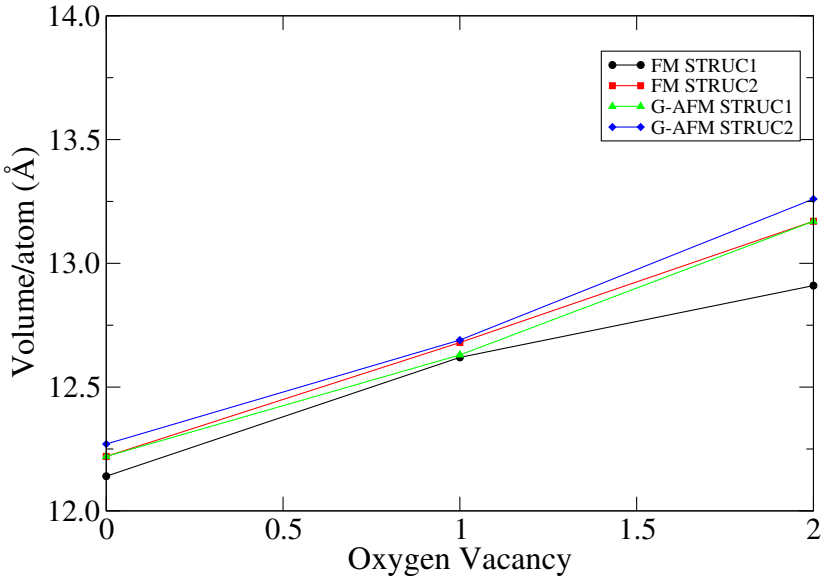

Figure 36: Volume per atom vs. number of vacancies for FM and G-AFM in STRUC1 and STRUC2 ordering.

Table 15 summarises the most striking vacancy features. This is done for the STRUC2 La-Sr distribution although -as discussed in detail above- there is no significant difference between the two distributions with respect to the vacancy properties. The first two columns shows again typical vacancy formation energies for the the FM and G-AFM ordering. Clearly, formation of a vacancy, being it single or pairwise, is significantly more costly in the FM case. It should however be noted -as also discussed above- that for the perfect state the FM case is more stable. This can be read from the last column in Table 15 listing the direct total energy difference between the two magnetic orderings. The first line is the difference between the perfect cases and shows a negative sign: FM is more stable than GAFM by 440 eV comparing unit cells with 40 atoms. The situation chnages, however, when vacancies are introduced: then the direct comparison of total energies in the last column clearly shows the preference for the G-AFM ordering. The value of the difference gets more than doubled for the vacancy pairs. Therefore, just considering the discussed theromodynamical ground states, the FM stable ordering can be changed into an G-AFM ordering when vacancies are

introduced. How this can be achieved experimentally is hard to figure out, but the present finding anyway deserves closer investigation in a future work.

Vacancy	$\Delta E_{form}^{\text{O-vac}}$ (eV)		ΔE (eV)
	FM	G-AFM	FM - G-AFM (eV)
0	0	0	-0.440
1	+1.086	-0.026	+0.750
2 short dist.	+1.342	+0.124	+1.990
2 long dist.	+1.617	+0.189	+2.413

Table 15: Summary of the vacancy calculations for the STRUC2 of $La_4Sr_4Fe_8O_{24-x}$ with x=1,2 for FM and G-AFM magnetic ordering. First two columns show the vacancy formation energy $\Delta E_{form}^{\text{O-vac}}$ per vacancy for both orderings, whereas the last column contains the direct difference ΔE between the total energies of the two different magnetic orderings.

8 Conclusion

This study deals with perovskite ferrates which are of interest as materials for solid oxide fuel cells. First-principles calculations within density functional theory are applied for describing and understanding properties such as formation energies of oxygen vacancies, the chemical bonding and related materials properties. The present work presents results of DFT calculations on perovskite ferrates such as $LaFeO_3$, $SrFeO_3$, and $La_{0.5}Sr_{0.5}FeO_3$. A particular problem for DFT modeling of these materials is the localized nature of the Fe-3d valence states which in this work are treated within the so-called DFT+U framework.

The perfect $LaFeO_3$ compound without vacancy was studied extensively and several magnetic orderings including FM and two types of AFM ordering were investigated. It turned out that the so-called G-AFM ordering is the most stable one for $LaFeO_3$. Different to the La-compound, the perfect compound of $SrFeO_3$ prefers FM ordering. Consequently, for the mixed case of $La_{0.5}Sr_{0.5}FeO_3$ FM as well as G-AFM ordering were taken into account. The distribution of Sr and La in the mixed compound was studied for two specific choices. Depending on the type of AFM larger unit cells have to be constructed. Finally a cell of composition $X_8Fe_8O_{24}$ (X=La,Sr) was taken into account, which allows the study of G-AFM as well as a reasonably small concentration of oxygen vacancies.

The study on single and double oxygen vacancies is treated in the final chapter. Extensive studies on all symmetrically different single vacancy sites in G-AFM $La_8Fe_8O_{24}$ were made revealing very costly vacancy formation energies of about 4.2 eV. The situation becomes very different for a single vacancy in $Sr_8Fe_8O_{24}$, which costs only about 0.3 eV. The highlight of the present work is the study of single and double vacancies in the mixed compounds $La_4Sr_4Fe_8O_{24}$ with their two different distributions of La and Sr. In general, the formation energies do not depend strongly on the specific La-Sr distribution but they are much more sensitive to magnetic ordering. For the FM ordering of the mixed case the vacancy formation energies are about 1 eV but they are much smaller for the G-AFM ordering, namely about 0.1 eV per vacancy. There are even cases with negative formation energies, which would mean that the perfect compound is not stable against the liberation of O_2 molecules. Introducing now vacancies the case with G-AFM ordering gets thermodynamically more stable than the mixed case in FM ordering, which is in contrast to the perfect compound. A further interesting finding for the G-AFM ordering with double vacancies is, that the compound is insulating with a gap larger than 1 eV. This feature corresponds to simple electron counting when all Fe ions have charge +3. Also very interesting is the occurence of a small gap for the FM ordering and two vacancies. This is one of the rare cases of a ferromagnetic insulating or semiconducting material. Summarising, the results on vacancies reveal very interesting physical properties and corroborate from first-principles the experimentally known fact that

La-Sr mixed ferrates produce a large numer of vacancies and free oxygen for the transport.

9 Appendix

9.1 POSCAR Example for Ferromagnetic cubic $LaFeO_3$

```
 bcc:
 -57.7992
        1.0000000000         0.0000000000         0.0000000000
        0.0000000000         1.0000000000         0.0000000000
        0.0000000000         0.0000000000         1.0000000000
   La   Fe    O
    1    1    3
Direct
    0.000000000        0.000000000         0.000000000 #La
    0.500000000        0.500000000         0.500000000 #Fe
    0.500000000        0.000000000         0.500000000 #O
    0.500000000        0.500000000         0.000000000 #O
    0.000000000        0.500000000         0.500000000 #O
```

9.2 INCAR Example for A-AFM tetragonal $La_2Fe_2O_6$

```
SYSTEM = LaFeO3 AFM
PREC = Accurate
LREAL = A        # faster but slightly different energies
ALGo = F
ISPIN=2
MAGMOM=2*0. 1*3. 1*-3. 6*0.
ISMEAR = 0
SIGMA = 0.05        # smaller sigma (default 0.2)
EDIFF=1E-6
ENCUT=600.0
LORBIT=10
LDAU=.TRUE.
LASPH = .TRUE.
LMAXMIX = 6
LDAUTYPE = 2
LDAUL = -1 2 -1
LDAUU = 0 6 0
LDAUJ = 0 1 0
```

```
LDAUPRINT = 1
NSW = 20
IBRION = 1
ISIF = 3
POTIM = 0.5
```

9.3 Orthorombic Distortion $LaFeO_3$

```
LaFeO3 DIST
    3.94810000000000
    2.0105672915749175    0.0000000000000000    0.0101503862943683
    0.0000000000000000    2.0058184675267294    0.0000000000000000
    0.0101584222058491    0.0000000000000000    2.0100893360688499
```

9.4 Oxygen Vacancy Calculations for $LaFeO_3$

```
 LaFeO3 DIST
3.94810000000000
  2.0105672915749175    0.0000000000000000    0.0101503862943683
  0.0000000000000000    2.0058184675267294    0.0000000000000000
  0.0101584222058491    0.0000000000000000    2.0100893360688499
   Fe   La   O
   8    8    24
Selective dynamics
  Direct
0.9986607627052329  0.0001075141231471  0.0004323892311536  # Fe
0.4986190747806782  0.9999534942863362  0.0003060809135309  # Fe
0.9986607627052329  0.4998924858768529  0.0004323892311536  # Fe
7.4986190747806782  0.5000465057136709  0.0003060809135309  # Fe
0.9989934374219257  0.0000526967517535  0.5004589793165112  # Fe
0.4989178815470582  0.9998991063311604  0.5003367276196167  # Fe
0.9989934374219257  0.4999473032482465  0.5004589793165112  # Fe
0.4989178815470582  0.5001008936688396  0.5003367276196167  # Fe
0.2724707067482517  0.2500000000000000  0.2645238200620606  # La
0.7640328962102779  0.2500000000000000  0.2742711511761623  # La
0.7341620781271158  0.7500000000000000  0.2272785792500009  # La
0.2253568985161576  0.7500000000000000  0.2350387321579862  # La
```

```
0.2631364249478527  0.2500000000000000  0.7728595386839709  # La
0.7714463051004395  0.2500000000000000  0.7659606398469403  # La
0.7255541762322903  0.7500000000000000  0.7360665289478519  # La
0.2335614406449636  0.7500000000000000  0.7271527830048909  # La
0.2489125392694833  0.0427412488980693  0.0376908030988182  # O 1
0.7482131208938556  0.9571761741788344  0.9630731856451253  # O 2
0.9481789299998050  0.2500000000000000  0.0319909134192627  # O 3
0.5280269458703406  0.2500000000000000  0.9484011840161599  # O 4
0.2489125392694833  0.4572587511019306  0.0376908030988182  # O 5
0.7482131208938556  0.5428238258211656  0.9630731856451253  # O 6
0.0484060920459102  0.7500000000000000  0.9688958732554003  # O 7
0.4685846773455591  0.7500000000000000  0.0522616522685606  # O 8
0.9616043111387637  0.9558081893228171  0.2502493833979553  # O 9
0.5356537720877677  0.0446683700591068  0.2507487843190288  # O 10
0.9616043111387637  0.5441918106771829  0.2502493833979553  # O 11
0.5356537720877677  0.4553316299408932  0.2507487843190288  # O 12
0.2485618286817018  0.9550049536777134  0.4637054404544440  # O 13
0.7492371932577587  0.0450092011391344  0.5372536287968152  # O 14
0.0311659474225227  0.2500000000000000  0.4489487228770737  # O 15
0.4467953256726948  0.2500000000000000  0.5314812221587818  # O 16
0.2485618286817018  0.5449950463222866  0.4637054404544440  # O 17
0.7492371932577587  0.4549907988608656  0.5372536287968152  # O 18
0.9671488083380435  0.7500000000000000  0.5520419247187224  # O 19
0.5514253953760276  0.7500000000000000  0.4692084758352654  # O 20
0.0357245648480646  0.0442803721552643  0.7507228395454261  # O 21
0.4618824581390956  0.9553091834063662  0.7499419406105937  # O 22
0.0357245648480646  0.4557196278447357  0.7507228395454261  # O 23
0.4618824581390956  0.5446908165936338  0.7499419406105937  # O 24
```

Oxygen Vacancy Sites	a [Å]	$\Delta E_{form}^{\text{O-vac}}$
18	3.961	4.1949
19	3.960	4.1843
20	3.962	4.1964
21	3.962	4.2001
22	3.960	4.1699
23	3.960	4.2006
24	3.960	4.2267
25	3.962	4.1987
26	3.960	4.1800
27	3.960	4.1819

9.5 Example of the Fortran Results

```
Atomic positions:
 -----------------
 atom types =   28
      total =   40
       lattice coordinates              (scaled) Cartesian coordinates
atom
 atom type   1:  atomic identification number = 26.0     representative =   1
 -0.002772  0.000016  0.002026           -0.005581  0.000032  0.004078      1
 -0.002772  0.499984  0.002026           -0.005581  1.006518  0.004078      3
 atom type   2:  atomic identification number = 26.0     representative =   2
 -0.498205 -0.000746 -0.000563           -1.002937 -0.001501 -0.001134      2
 -0.498205 -0.499254 -0.000563           -1.002937 -1.005049 -0.001134      4
 atom type   3:  atomic identification number = 26.0     representative =   5
  0.001145 -0.000072  0.498698            0.002305 -0.000145  1.003928      5
  0.001145 -0.499928  0.498698            0.002305 -1.006405  1.003928      7
 atom type   4:  atomic identification number = 26.0     representative =   6
  0.499593 -0.000328 -0.499316            1.005730 -0.000660 -1.005174      6
  0.499593 -0.499672 -0.499316            1.005730 -1.005890 -1.005174      8
 atom type   5:  atomic identification number = 57.0     representative =   9
  0.247146  0.250000  0.252817            0.497530  0.503275  0.508946      9
 atom type   6:  atomic identification number = 57.0     representative =  10
 -0.248321 -0.250000  0.246646           -0.499894 -0.503275  0.496523     10
 atom type   7:  atomic identification number = 57.0     representative =  11
```

```
 0.252463 -0.250000 -0.252855            0.508233 -0.503275 -0.509023     11
atom type   8:  atomic identification number = 57.0     representative =  12
-0.251696  0.250000 -0.247283          -0.506690  0.503275 -0.497805     12
atom type   9:  atomic identification number = 38.0     representative =  13
-0.250181  0.250000  0.247631          -0.503639  0.503275  0.498506     13
atom type  10:  atomic identification number = 38.0     representative =  14
 0.252766 -0.250000  0.251886            0.508844 -0.503275  0.507072     14
atom type  11:  atomic identification number = 38.0     representative =  15
 0.248446  0.250000 -0.252314            0.500146  0.503275 -0.507934     15
atom type  12:  atomic identification number = 38.0     representative =  16
-0.247991 -0.250000 -0.247593          -0.499232 -0.503275 -0.498429     16
atom type  13:  atomic identification number =  8.0     representative =  17
 0.247529  0.020208  0.018831            0.498301  0.040680  0.037909     17
 0.247529  0.479792  0.018831            0.498301  0.965870  0.037909     21
atom type  14:  atomic identification number =  8.0     representative =  18
-0.251231  0.000591 -0.006069          -0.505754  0.001189 -0.012218     18
-0.251231  0.499409 -0.006069          -0.505754  1.005361 -0.012218     22
atom type  15:  atomic identification number =  8.0     representative =  19
-0.003116  0.250000  0.003598          -0.006272  0.503275  0.007243     19
atom type  16:  atomic identification number =  8.0     representative =  20
-0.493800  0.250000 -0.022296          -0.994068  0.503275 -0.044884     20
atom type  17:  atomic identification number =  8.0     representative =  23
 0.023956 -0.250000 -0.016956            0.048227 -0.503275 -0.034134     23
atom type  18:  atomic identification number =  8.0     representative =  24
 0.499498 -0.250000  0.006976            1.005539 -0.503275  0.014043     24
atom type  19:  atomic identification number =  8.0     representative =  25
-0.021075 -0.022126  0.249728          -0.042427 -0.044542  0.502728     25
-0.021075 -0.477874  0.249728          -0.042427 -0.962008  0.502728     27
atom type  20:  atomic identification number =  8.0     representative =  26
-0.494012  0.002722  0.250241          -0.994496  0.005479  0.503760     26
-0.494012  0.497278  0.250241          -0.994496  1.001071  0.503760     28
atom type  21:  atomic identification number =  8.0     representative =  29
 0.251174 -0.000218  0.495530            0.505638 -0.000439  0.997552     29
 0.251174 -0.499782  0.495530            0.505638 -1.006111  0.997552     33
atom type  22:  atomic identification number =  8.0     representative =  30
-0.249625  0.020939 -0.479620          -0.502519  0.042152 -0.965523     30
-0.249625  0.479061 -0.479620          -0.502519  0.964398 -0.965523     34
```

```
atom type  23:  atomic identification number =  8.0     representative =  31
 0.018380  0.250000  0.481884            0.037001  0.503275  0.970080     31
atom type  24:  atomic identification number =  8.0     representative =  32
 0.497491  0.250000 -0.498062            1.001499  0.503275 -1.002648     32
atom type  25:  atomic identification number =  8.0     representative =  35
 0.000141 -0.250000 -0.494459            0.000284 -0.503275 -0.995396     35
atom type  26:  atomic identification number =  8.0     representative =  36
-0.482484 -0.250000  0.482289           -0.971289 -0.503275  0.970896     36
atom type  27:  atomic identification number =  8.0     representative =  37
 0.004232  0.001354 -0.249760            0.008520  0.002726 -0.502792     37
 0.004232  0.498646 -0.249760            0.008520  1.003824 -0.502792     39
atom type  28:  atomic identification number =  8.0     representative =  38
 0.480834 -0.022895 -0.250666            0.967966 -0.046090 -0.504616     38
 0.480834 -0.477105 -0.250666            0.967966 -0.960460 -0.504616     40
  atomic sphere information:
-------------------------
 atom kind 1 (Fe): sphere radius =  2.35
    minimum distances to other atom kinds
        1   Fe     7.38710 a.u.
        2   La    40.39333 a.u.
        3   Sr    40.55571 a.u.
        4   O      3.73011 a.u.
 atom kind 2 (La): sphere radius =  2.50
    minimum distances to other atom kinds
        2   La    10.52180 a.u.
        3   Sr     7.44328 a.u.
        4   O      4.80767 a.u.
 atom kind 3 (Sr): sphere radius =  2.50
    minimum distances to other atom kinds
        3   Sr    10.51688 a.u.
        4   O      5.18711 a.u.
 atom kind 4 (O ): sphere radius =  1.37
    minimum distances to other atom kinds
Neighbors for atom type 1 (Fe): (distances in a.u.)
 atom type 1 (Fe)
          7.442426     1        ( 3.938361 A)
          7.443379     1        ( 3.938865 A)
```

```
 atom type 2 (Fe)
           7.387102     1        ( 3.909084 A)
           7.522850     1        ( 3.980919 A)
 atom type 13 (O)
           4.641669     1        ( 2.456264 A)
           8.512394     1        ( 4.504563 A)
           9.023497     1        ( 4.775027 A)
 atom type 14 (O)
           3.928878     1        ( 2.079072 A)
           8.408240     1        ( 4.449447 A)
           8.424208     1        ( 4.457897 A)
 atom type 15 (O)
           3.730110     1        ( 1.973888 A)
 atom type 16 (O)
           9.117802     1        ( 4.824931 A)
           9.333314     1        ( 4.938975 A)
 atom type 17 (O)
           4.865187     1        ( 2.574545 A)
 atom type 18 (O)
           8.330839     1        ( 4.408489 A)
           8.391001     1        ( 4.440325 A)
Neighbors for atom type 2 (Fe): (distances in a.u.)
 atom type 1 (Fe)
           7.387102     1        ( 3.909084 A)
           7.522850     1        ( 3.980919 A)
 atom type 2 (Fe)
           7.420703     1        ( 3.926865 A)
           7.465103     1        ( 3.950361 A)
 atom type 13 (O)
           4.950552     1        ( 2.619718 A)
           8.693611     1        ( 4.600459 A)
           9.176272     1        ( 4.855872 A)
 atom type 14 (O)
           3.785403     1        ( 2.003148 A)
           8.348132     1        ( 4.417639 A)
           8.352249     1        ( 4.419818 A)
 atom type 15 (O)
```

```
           8.289166     1        ( 4.386436 A)
           8.419405     1        ( 4.455355 A)
 atom type 16 (O)
           5.157499     1        ( 2.729230 A)
 atom type 17 (O)
           8.459712     1        ( 4.476685 A)
           9.021547     1        ( 4.773995 A)
 atom type 18 (O)
           3.910472     1        ( 2.069332 A)
Neighbors for atom type 3 (Fe): (distances in a.u.)
 atom type 3 (Fe)
           7.440757     1        ( 3.937477 A)
           7.445049     1        ( 3.939749 A)
 atom type 4 (Fe)
           7.426918     1        ( 3.930154 A)
           7.473093     1        ( 3.954589 A)
 atom type 21 (O)
           3.757838     1        ( 1.988561 A)
           8.333898     1        ( 4.410107 A)
           8.341610     1        ( 4.414188 A)
 atom type 22 (O)
           5.161140     1        ( 2.731156 A)
           8.798240     1        ( 4.655826 A)
           9.308954     1        ( 4.926085 A)
 atom type 23 (O)
           4.637133     1        ( 2.453864 A)
 atom type 24 (O)
           8.290286     1        ( 4.387029 A)
           8.387382     1        ( 4.438410 A)
 atom type 25 (O)
           3.885492     1        ( 2.056113 A)
 atom type 26 (O)
           8.537495     1        ( 4.517846 A)
           8.952316     1        ( 4.737360 A)
Neighbors for atom type 4 (Fe): (distances in a.u.)
 atom type 3 (Fe)
           7.426918     1        ( 3.930154 A)
```

```
           7.473093     1        ( 3.954589 A)
 atom type 4 (Fe)
           7.433147     1        ( 3.933451 A)
           7.452658     1        ( 3.943775 A)
 atom type 21 (O)
           3.792975     1        ( 2.007155 A)
           8.346412     1        ( 4.416729 A)
           8.360889     1        ( 4.424390 A)
 atom type 22 (O)
           4.943457     1        ( 2.615964 A)
           8.675329     1        ( 4.590784 A)
           9.186711     1        ( 4.861396 A)
 atom type 23 (O)
           8.641411     1        ( 4.572836 A)
           9.110437     1        ( 4.821034 A)
 atom type 24 (O)
           3.732118     1        ( 1.974951 A)
 atom type 25 (O)
           8.349898     1        ( 4.418574 A)
           8.364441     1        ( 4.426270 A)
 atom type 26 (O)
           4.791286     1        ( 2.535438 A)
Neighbors for atom type 5 (La): (distances in a.u.)
 atom type 9 (Sr)
           7.451662     1        ( 3.943248 A)
           7.530718     1        ( 3.985083 A)
 atom type 10 (Sr)
           7.444934     2        ( 3.939688 A)
 atom type 19 (O)
           5.710218     2        ( 3.021716 A)
 atom type 20 (O)
           5.345400     2        ( 2.828663 A)
Neighbors for atom type 6 (La): (distances in a.u.)
 atom type 9 (Sr)
           7.444701     2        ( 3.939565 A)
 atom type 10 (Sr)
           7.476123     1        ( 3.956192 A)
```

```
           7.508269     1        ( 3.973203 A)
 atom type 19 (O)
           4.817028     2        ( 2.549061 A)
 atom type 20 (O)
           5.279666     2        ( 2.793878 A)
Neighbors for atom type 7 (La): (distances in a.u.)
 atom type 11 (Sr)
           7.443670     2        ( 3.939019 A)
 atom type 12 (Sr)
           7.485901     1        ( 3.961367 A)
           7.499343     1        ( 3.968480 A)
 atom type 27 (O)
           5.283029     2        ( 2.795657 A)
 atom type 28 (O)
           4.807671     2        ( 2.544109 A)
Neighbors for atom type 8 (La): (distances in a.u.)
 atom type 11 (Sr)
           7.486256     1        ( 3.961555 A)
           7.490462     1        ( 3.963780 A)
 atom type 12 (Sr)
           7.443280     2        ( 3.938813 A)
 atom type 27 (O)
           5.327094     2        ( 2.818976 A)
 atom type 28 (O)
           5.715002     2        ( 3.024248 A)
Neighbors for atom type 9 (Sr): (distances in a.u.)
 atom type 5 (La)
           7.451662     1        ( 3.943248 A)
           7.530718     1        ( 3.985083 A)
 atom type 6 (La)
           7.444701     2        ( 3.939565 A)
 atom type 19 (O)
           5.306412     2        ( 2.808031 A)
 atom type 20 (O)
           5.187108     2        ( 2.744898 A)
Neighbors for atom type 10 (Sr): (distances in a.u.)
 atom type 5 (La)
```

```
          7.444934     2        ( 3.939688 A)
 atom type 6 (La)
          7.476123     1        ( 3.956192 A)
          7.508269     1        ( 3.973203 A)
 atom type 19 (O)
          5.314864     2        ( 2.812504 A)
 atom type 20 (O)
          5.332297     2        ( 2.821729 A)
Neighbors for atom type 11 (Sr): (distances in a.u.)
 atom type 7 (La)
          7.443670     2        ( 3.939019 A)
 atom type 8 (La)
          7.486256     1        ( 3.961555 A)
          7.490462     1        ( 3.963780 A)
 atom type 27 (O)
          5.204811     2        ( 2.754266 A)
 atom type 28 (O)
          5.342417     2        ( 2.827084 A)
Neighbors for atom type 12 (Sr): (distances in a.u.)
 atom type 7 (La)
          7.485901     1        ( 3.961367 A)
          7.499343     1        ( 3.968480 A)
 atom type 8 (La)
          7.443280     2        ( 3.938813 A)
 atom type 27 (O)
          5.312460     2        ( 2.811232 A)
 atom type 28 (O)
          5.289292     2        ( 2.798972 A)
Neighbors for atom type 13 (O): (distances in a.u.)
 atom type 1 (Fe)
          4.641669     1        ( 2.456264 A)
          8.512394     1        ( 4.504563 A)
          9.023497     1        ( 4.775027 A)
 atom type 2 (Fe)
          4.950552     1        ( 2.619718 A)
          8.693611     1        ( 4.600459 A)
          9.176272     1        ( 4.855872 A)
```

```
 atom type 13 (O)
           6.841286     1        ( 3.620251 A)
           8.044520     1        ( 4.256975 A)
 atom type 14 (O)
           8.475374     1        ( 4.484973 A)
           8.507715     1        ( 4.502087 A)
 atom type 15 (O)
           5.642979     1        ( 2.986135 A)
 atom type 16 (O)
           8.478065     1        ( 4.486397 A)
 atom type 17 (O)
           7.848134     1        ( 4.153052 A)
 atom type 18 (O)
           5.832234     1        ( 3.086284 A)
Neighbors for atom type 14 (O): (distances in a.u.)
 atom type 1 (Fe)
           3.928878     1        ( 2.079072 A)
           8.408240     1        ( 4.449447 A)
           8.424208     1        ( 4.457897 A)
 atom type 2 (Fe)
           3.785403     1        ( 2.003148 A)
           8.348132     1        ( 4.417639 A)
           8.352249     1        ( 4.419818 A)
 atom type 13 (O)
           8.475374     1        ( 4.484973 A)
           8.507715     1        ( 4.502087 A)
 atom type 14 (O)
           7.425323     1        ( 3.929310 A)
           7.460483     1        ( 3.947916 A)
 atom type 15 (O)
           5.470904     1        ( 2.895077 A)
 atom type 16 (O)
           5.820783     1        ( 3.080224 A)
 atom type 17 (O)
           5.820045     1        ( 3.079834 A)
 atom type 18 (O)
           5.678564     1        ( 3.004965 A)
```

```
Neighbors for atom type 15 (O): (distances in a.u.)
 atom type 1 (Fe)
           3.730110     2        ( 1.973888 A)
 atom type 2 (Fe)
           8.289166     2        ( 4.386436 A)
           8.419405     2        ( 4.455355 A)
 atom type 13 (O)
           5.642979     2        ( 2.986135 A)
 atom type 14 (O)
           5.470904     2        ( 2.895077 A)
 atom type 16 (O)
           8.445639     1        ( 4.469238 A)
           8.686621     1        ( 4.596760 A)
 atom type 17 (O)
           8.178412     2        ( 4.327828 A)
Neighbors for atom type 16 (O): (distances in a.u.)
 atom type 1 (Fe)
           9.117802     2        ( 4.824931 A)
           9.333314     2        ( 4.938975 A)
 atom type 2 (Fe)
           5.157499     2        ( 2.729230 A)
 atom type 13 (O)
           8.478065     2        ( 4.486397 A)
 atom type 14 (O)
           5.820783     2        ( 3.080224 A)
 atom type 15 (O)
           8.445639     1        ( 4.469238 A)
           8.686621     1        ( 4.596760 A)
 atom type 18 (O)
           8.853258     2        ( 4.684940 A)
Neighbors for atom type 17 (O): (distances in a.u.)
 atom type 1 (Fe)
           4.865187     2        ( 2.574545 A)
 atom type 2 (Fe)
           8.459712     2        ( 4.476685 A)
           9.021547     2        ( 4.773995 A)
 atom type 13 (O)
```

```
           7.848134     2        ( 4.153052 A)
 atom type 14 (O)
           5.820045     2        ( 3.079834 A)
 atom type 15 (O)
           8.178412     2        ( 4.327828 A)
 atom type 18 (O)
           8.091102     1        ( 4.281625 A)
           8.735301     1        ( 4.622520 A)
Neighbors for atom type 18 (O): (distances in a.u.)
 atom type 1 (Fe)
           8.330839     2        ( 4.408489 A)
           8.391001     2        ( 4.440325 A)
 atom type 2 (Fe)
           3.910472     2        ( 2.069332 A)
 atom type 13 (O)
           5.832234     2        ( 3.086284 A)
 atom type 14 (O)
           5.678564     2        ( 3.004965 A)
 atom type 16 (O)
           8.853258     2        ( 4.684940 A)
 atom type 17 (O)
           8.091102     1        ( 4.281625 A)
           8.735301     1        ( 4.622520 A)
Neighbors for atom type 19 (O): (distances in a.u.)
 atom type 5 (La)
           5.710218     1        ( 3.021716 A)
 atom type 6 (La)
           4.817028     1        ( 2.549061 A)
 atom type 9 (Sr)
           5.306412     1        ( 2.808031 A)
 atom type 10 (Sr)
           5.314864     1        ( 2.812504 A)
 atom type 19 (O)
           6.784170     1        ( 3.590027 A)
           8.101636     1        ( 4.287199 A)
 atom type 20 (O)
           7.050254     1        ( 3.730832 A)
```

```
          7.854926     1        ( 4.156646 A)
Neighbors for atom type 20 (O): (distances in a.u.)
 atom type 5 (La)
          5.345400     1        ( 2.828663 A)
 atom type 6 (La)
          5.279666     1        ( 2.793878 A)
 atom type 9 (Sr)
          5.187108     1        ( 2.744898 A)
 atom type 10 (Sr)
          5.332297     1        ( 2.821729 A)
 atom type 19 (O)
          7.050254     1        ( 3.730832 A)
          7.854926     1        ( 4.156646 A)
 atom type 20 (O)
          7.361869     1        ( 3.895732 A)
          7.523937     1        ( 3.981494 A)
Neighbors for atom type 21 (O): (distances in a.u.)
 atom type 3 (Fe)
          3.757838     1        ( 1.988561 A)
          8.333898     1        ( 4.410107 A)
          8.341610     1        ( 4.414188 A)
 atom type 4 (Fe)
          3.792975     1        ( 2.007155 A)
          8.346412     1        ( 4.416729 A)
          8.360889     1        ( 4.424390 A)
 atom type 21 (O)
          7.436410     1        ( 3.935177 A)
          7.449396     1        ( 3.942049 A)
 atom type 22 (O)
          8.477960     1        ( 4.486342 A)
          8.498796     1        ( 4.497367 A)
 atom type 23 (O)
          5.556530     1        ( 2.940388 A)
 atom type 24 (O)
          5.330902     1        ( 2.820991 A)
 atom type 25 (O)
          5.520484     1        ( 2.921313 A)
```

```
 atom type 26 (O)
           5.851931     1        ( 3.096707 A)
Neighbors for atom type 22 (O): (distances in a.u.)
 atom type 3 (Fe)
           5.161140     1        ( 2.731156 A)
           8.798240     1        ( 4.655826 A)
           9.308954     1        ( 4.926085 A)
 atom type 4 (Fe)
           4.943457     1        ( 2.615964 A)
           8.675329     1        ( 4.590784 A)
           9.186711     1        ( 4.861396 A)
 atom type 21 (O)
           8.477960     1        ( 4.486342 A)
           8.498796     1        ( 4.497367 A)
 atom type 22 (O)
           6.819520     1        ( 3.608733 A)
           8.066285     1        ( 4.268493 A)
 atom type 23 (O)
           8.202236     1        ( 4.340435 A)
 atom type 24 (O)
           5.908958     1        ( 3.126884 A)
 atom type 25 (O)
           5.999454     1        ( 3.174773 A)
 atom type 26 (O)
           8.196565     1        ( 4.337434 A)
Neighbors for atom type 23 (O): (distances in a.u.)
 atom type 3 (Fe)
           4.637133     2        ( 2.453864 A)
 atom type 4 (Fe)
           8.641411     2        ( 4.572836 A)
           9.110437     2        ( 4.821034 A)
 atom type 21 (O)
           5.556530     2        ( 2.940388 A)
 atom type 22 (O)
           8.202236     2        ( 4.340435 A)
 atom type 24 (O)
           7.851633     1        ( 4.154904 A)
```

```
          8.420544     1        ( 4.455958 A)
 atom type 25 (O)
          8.395011     2        ( 4.442447 A)
Neighbors for atom type 24 (O): (distances in a.u.)
 atom type 3 (Fe)
          8.290286     2        ( 4.387029 A)
          8.387382     2        ( 4.438410 A)
 atom type 4 (Fe)
          3.732118     2        ( 1.974951 A)
 atom type 21 (O)
          5.330902     2        ( 2.820991 A)
 atom type 22 (O)
          5.908958     2        ( 3.126884 A)
 atom type 23 (O)
          7.851633     1        ( 4.154904 A)
          8.420544     1        ( 4.455958 A)
 atom type 26 (O)
          8.114037     2        ( 4.293762 A)
Neighbors for atom type 25 (O): (distances in a.u.)
 atom type 3 (Fe)
          3.885492     2        ( 2.056113 A)
 atom type 4 (Fe)
          8.349898     2        ( 4.418574 A)
          8.364441     2        ( 4.426270 A)
 atom type 21 (O)
          5.520484     2        ( 2.921313 A)
 atom type 22 (O)
          5.999454     2        ( 3.174773 A)
 atom type 23 (O)
          8.395011     2        ( 4.442447 A)
 atom type 26 (O)
          8.130784     1        ( 4.302624 A)
          8.591257     1        ( 4.546296 A)
Neighbors for atom type 26 (O): (distances in a.u.)
 atom type 3 (Fe)
          8.537495     2        ( 4.517846 A)
          8.952316     2        ( 4.737360 A)
```

```
 atom type 4 (Fe)
           4.791286     2        ( 2.535438 A)
 atom type 21 (O)
           5.851931     2        ( 3.096707 A)
 atom type 22 (O)
           8.196565     2        ( 4.337434 A)
 atom type 24 (O)
           8.114037     2        ( 4.293762 A)
 atom type 25 (O)
           8.130784     1        ( 4.302624 A)
           8.591257     1        ( 4.546296 A)
Neighbors for atom type 27 (O): (distances in a.u.)
 atom type 7 (La)
           5.283029     1        ( 2.795657 A)
 atom type 8 (La)
           5.327094     1        ( 2.818976 A)
 atom type 11 (Sr)
           5.204811     1        ( 2.754266 A)
 atom type 12 (Sr)
           5.312460     1        ( 2.811232 A)
 atom type 27 (O)
           7.402593     1        ( 3.917282 A)
           7.483213     1        ( 3.959944 A)
 atom type 28 (O)
           7.105321     1        ( 3.759973 A)
           7.800980     1        ( 4.128099 A)
Neighbors for atom type 28 (O): (distances in a.u.)
 atom type 7 (La)
           4.807671     1        ( 2.544109 A)
 atom type 8 (La)
           5.715002     1        ( 3.024248 A)
 atom type 11 (Sr)
           5.342417     1        ( 2.827084 A)
 atom type 12 (Sr)
           5.289292     1        ( 2.798972 A)
 atom type 27 (O)
           7.105321     1        ( 3.759973 A)
```

```
          7.800980     1        ( 4.128099 A)
atom type 28 (O)
          6.761283     1        ( 3.577915 A)
          8.124523     1        ( 4.299311 A)
```

9.6 Double Oxygen Vacancy Calculations for $SrLaFeO_3$ in G-AFM: STRUC1

Double Vacancies	$\Delta E_{form}^{\text{O-vac}}$ (eV)
short dist. at 17-26	-0.417
long dist. at 17-31	0.118
short dist. at 25-18	-0.411
long dist. at 25-20	-0.1

9.7 Oxygen Vacancy Calculations for $SrLaFeO_3$ in G-AFM: STRUC2

Oxygen Vacancy Sites	$\Delta E_{form}^{O\text{-}vac}$ (eV)
17	-0.057883
18	-0.128533
19	-0.126253
20	-0.057883
21	-0.128533
22	-0.126253
23	-0.054293
24	-0.118823
25	0.410777
26	-0.123603
27	-0.010103
28	-0.125373
29	-0.126033
30	0.418337
31	-0.056763
32	-0.126713
33	-0.126033
34	-0.053973
35	0.580327
36	0.487317
37	-0.755103
38	-0.056013
39	-0.120393
40	-0.048653

9.8 Oxygen Vacancy Calculations for $SrLaFeO_3$ in FM: STRUC2

Oxygen Vacancy Sites	$\Delta E_{form}^{\text{O-vac}}$ (eV)
17	1.119127
18	1.026247
20	1.221657
21	1.147937
23	1.179627
24	0.996437
25	1.021897
26	1.020857
27	1.139087
28	1.021827
29	1.017877
30	1.143447
31	1.198257
32	0.995547
33	1.017147
34	1.155347
35	0.995167
36	1.220727
37	1.023517
39	1.023357
40	1.138967

References

[1] URL: http://foxsi.tuwien.ac.at/

[2] E. Perry Murray, T. Tsai, S. A. Barnett, **400**, 649-651 (1999).

[3] E. V. Tsipis, V. V. Kharton, **12**, 1367-1391, (2008).

[4] M. Liu, E. M. Lynch, K. Blinn, F. M. Alamgir, Y. Choi, **14**, 534-546, (2011).

[5] S. P. S. Badwal, Solid State Ionics, **143**, 39-46 (2001).

[6] S. B. Adler, Chem. Rev., 104, 4791-4843, (2004).

[7] B. C. Steele, H. Heinzel, A. Nature **414**, 345-352 (2011).

[8] A. M. Ritzmann, A. B. Muñ*oz – García*, M. Pavone, J. A. Keith, E. A. Carter, Chem. Mater., **25 (15)**, 30113019, (2013).

[9] Z. Lu, J. Hardy, J. Templeton, J. Stevenson, Power Sources, **198**, 90-94 (2012).

[10] URL: http://www.netl.doe.gov/technologies/coalpower/fuelcells/seca/pubs/SECA-Fuel-Cell-Cathode-Research-2007-2013.pdf

[11] A. B. Muñ*oz – García*, D. E. Bugaris, M. Pavone, J. P. Hodges, A. Huq, F. Chen, H. C. zur Loye and E. A. Carter, J. Am. Chem. Soc., **134**, 68266833 (2012).

[12] M. Pavone, A. M. Ritzmann, E. A. Carter, The Royal Society of Chemistry, **10**, 1039, (2011).

[13] P. Patnaik, Handbook of Inorganic Chemicals, McGraw-Hill, 444-446, (2003).

[14] W. Chen, T. Saito, N.Hayashi, M. Takano, Y. Shimakawa, Scientific Reports 2, **449**, (2012).

[15] I. R. Shein, K.I. Shein, V. L. Kozhevnikov, A. L. Ivanovskii, Physics of the Solid State **47** 2082 (2005).

[16] P. Hohenberg and W. Kohn, Phys. Rev. **136**, B864 (1964).

[17] L.J. Sham and W. Kohn, Phys. Rev. B **140**, A1133 (1965).

[18] J.P. Perdew, K. Burke and M. Ernzerhof, Phys. Rev. Lett., **77**, 3865 (1996).

[19] P. Bloechl, Phy. Rev. B., **50**, 17953-17973, (1994).

[20] G. Kresse and J. Hafner, Phys. Rev. B, **47** 558, (1993).

[21] G. Kresse and J. Hafner, Phys. Rev. B, **49** 14251, (1994).

[22] G. Kresse and J. Furthmller, Comput. Mat. Sci., **6** 15, (1996).

[23] Monkhorst, J. Hendrik and Pack, D. James,Phys. Rev. B, **13**, 5188, (1976).

[24] S. L. Dudarev, G. A. Botton, S. Y. Savrasov, C. J. Humphreys and A. P. Sutton, Phys. Rev. B **57**, 1505, (1998).

[25] Lecture of R. Podloucky, Chemische Bindung und Eigenschaften fester Materie, Summer Semester, (2013).

[26] A. M. Ritzmann, A. B. *Muñoz – García*,, M. Pavone, J. A. Keith and E. A. Carter, **3**, 161-166, (2013).

[27] J. Richter, P. Holtappels, T. Graule, T. Nakamura, L. J. Gauckler, Springer-Verlag, **140**, 985-999 (2009).

[28] H. L. Lukas, S. G. Fries and B. Sundman, Computational Thermodynamics, the Calphad Method, Cambridge University Press, (2007).

[29] URL: http://cms.mpi.univie.ac.at/vasp/guide/node112.html

[30] Internship study performed under supervision of J. Redinger, Vienna University of Technology, 2013 Vienna University of Technology Center for Computational Materials Science, (2012-2013)

[31] W. C. Koehler and E. O. Wollan, J. Phys. Chem. Solids. Pergamon Press **2** 100-106 (1957)

[32] T. Arima and Y. Tokura, Physical Review B, **48**, 23, (1993)

[33] H. Wadati, D. Kobayashi, H. Kumigashira, K. Okazaki, T. Mizokawa, A. Fujimori, K. Horiba, M. Oshima, N. Hamada, M. Lipmaa, M. Kawasaki, and H. Koinuma, Physical Review B **71**, (2005)

[34] I. Solovyev, N. Hamada, and K. Terakura, Phy. Rev. B, **53**, 7158, (1996)

[35] A.E. Bocquet, S.Suga, N.Kimizuka, Y. Takeda, Takano, Physical Review B (Condensed Matter), **45**, 1561-1570, (1992)

[36] T. Takeda, S. Komura, and N. Watanabe, Proceedings of the International Conference, Japan, (1980)

[37] D. D. Sarma, N Shanti, S. R. Barman, N Hamada, H Sawada, K. Terakura, K. Phys. Rev. Lett. **75**, (1126-1129).

[38] P. Mahadevan, N. Shanthi, D. D. Sarma, J. Phy, Condens Matter, **9**, 3129-3138, (1997)

[39] flair: https://pantherfile.uwm.edu/weinert/www/flair.html

[40] T. Ishigaki, S. Yamauchi, J. Mizusaki, and K. Fueki, J. Solid State Chem, **54**, 100-107 (1984).

[41] T. Ishigaki, S. Yamauchi, J. Mizusaki, and K. Kishio, J. Mizusaki, J. Solid State Chem, **73**, 179-187 (1988).

[42] Z. Zeng, F. Calle-Vallejo, M. B. Mogensen and J. Rossmeisl, **15**, 7526, 2013.

Curriculum Vitae

Personal Data

Name:	Zeynep Ergönenc
Date of birth and place:	30.04.1987, Ankara, TURKEY
Nationality:	Turkish
Gender:	Female
E-mail:	ergonenc.zeynep@gmail.com
Civil Status:	Single
Address:	Lerchengasse 27/7 1080 Vienna/Austria
Phone:	069919098519

Education

2011-2014:	Master of Chemistry at the University of Vienna
Oct, 2012-March, 2013:	Internship at Institute de Ciéncia de Materials de Barcelona
August, 2013:	Summer School on Materials in 3D, at The UCSB
2005-2006:	Hacettepe University School of Foreign Languages, English
2005-2010:	Bachelor of Chemistry at the Hacettepe University
March, 2009-Oct, 2010:	Study abroad (Erasmus) at the University of Bremen
2001-2002:	Ankara Anatolian High School of Foreign Languages, German
2001-2005:	Mathematics-Natural Sciences, Ankara Anatolian High School